Study of plasma fluctuations in conventional torch

2.1 Introduction

The previous chapter has shown the coatings production by the suspension plasma spraying method and its advantages, i.e. the simplicity, low cost, wide range of the materials. However, there are still many difficulties encountered by the researchers working on this method. The problem with sufficient reproducibility and reliability, due to e.g. the plasma instabilities, is the reason why for many years the special efforts have been devoted to improve this method. This development process requires the profound studies of the plasma instabilities produced by a torch. Therefore, the purpose of the following chapter is to understand the origins of the arc fluctuations. The measurements will be performed by using the conventional dc plasma torch, which will be described in the following paragraph. The time-resolved measurements and the data processing methods will be presented. This kind of experimental procedure applied to the arc voltage signal has leaded to determine a mode due to Helmholtz resonance in the torch, what will be described and investigated in the following chapter. The presented profound studies of the resonance in the torch and described in the previous chapter restrike fluctuations will result in a new resonant mode in the dc plasma torch.

2.1.1 Plasma torch

All measurements have been carried out at atmospheric pressure using a home-made plasma torch, shown schematically in Figure 2.1. It presents a similar configuration as the commercial F4 gun (Sulzer Metco, Switzerland). The torch consists of the nozzle with the variable diameter, d, which in the performed experiments will be chosen between 6 mm and 8 mm. The swirl gas injection is obtained by the injection ring with 16 holes of diameter 1 mm. The geometrical parameters of the torch are indicated in Figure 2.1. The volume of the cathode cavity, V_g, corresponds to the space limited by the injection ring up to the cathode tip. V_g and the distance between the end of cathode and the nozzle exit, L_k, are variable, what is shown in Table 2.1.

It presents the configurations of V_g and L_k used in the experiments. It is possible to choose the cathode cavity volume between: $V_g = 6$ cm^3, which corresponds to the standard volume, $V_g = 8.7$ cm^3, obtained by removing the injection ring and $V_g = 12.5$ cm^3, volume of a cavity specially machined in the laboratory.

The torch is power supplied with a current regulated source (SNMI, type P130, open circuit voltage 180 V), that provides the current up to 1000 A with a maximum voltage of 100 V. The electrodes cooling system consists of the pump which can be operated at the pressure 1.6 MPa.

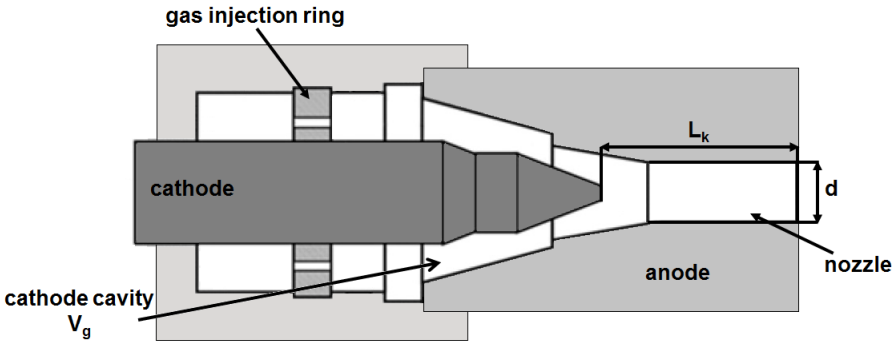

Figure 2.1: Schematic view of the torch.

Table 2.1: Configurations of the volume of cathode cavity and of the distance between cathode tip and the nozzle exit chosen in the experiments.

V_g	(cm^3)	6	8.7	12.5
L_k	(mm)	30	29.5	

The circulating water is delivered to the anode and cathode with an average flow rate of 17 l/min. The operation of the torch is characterized by mean values of the arc voltage ($\overline{V}$) and the arc current. The following paragraphs define the measurement methods of the process parameters.

2.1.1.1 Time-resolved measurements and data processing

The time-resolved measurements of the signals have been carried out using a data acquisition PCI 6132 computer card piloted by Labview software. This National Instruments card, which has 4 simultaneous recording channels (bandwidth 1.3 MHz, sampling rate 2.5 MS/s/channel, accuracy 14 bits), allows converting the signal from an analog to a digital form, by sampling and then digitizing it using an analog-to-digital converter (ADC). The sampling process is of critical importance in this kind of measurement. The resulting signal waveform is highly dependent on the sampling frequency. If this frequency is too low, aliasing occurs and the original analog signal is incorrectly reconstructed, what is presented in Figure 2.2 b).

To obtain the signal without aliasing, the Nyquist sampling criterion should be met. It shows that samples taken at a frequency, f_s, at least twice the highest frequency content of a signal, f_{max}, are sufficient for a correct reconstruction. In practice, f_s should be greater than f_{max} to obtain the original analog signal reconstructed exactly, what is presented as follows: $f_s > 2f_{max}$.

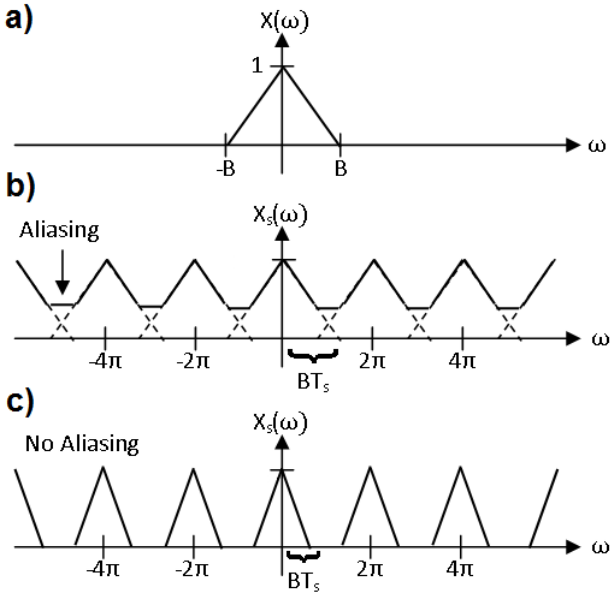

Figure 2.2: Results of the sampling frequency choice: a) original signal, b) sampling frequency below Nyquist frequency (resulting signal with aliasing), c) sampling above Nyquist frequency (no aliasing occurs) [68].

The signals have been recorded by LabView program for further data processing, e.g. the statistical analysis of the signals. To achieve the reliable values the results are the average of 10 measured signals.

The statistical analysis of the measured data gives the information about:

- Mean value

  Considering the recorded data as X the mean value is denoted by $\overline{X}$ and defined by the following formula:

$$\overline{X} = \frac{1}{n}\sum_{i=1}^{n} X_i \tag{2.1}$$

  where n = 6500 samples in the measurements performed in this work.

  To obtain the reliable values for each operating conditions the data contains 10 measurements. Therefore, the final mean value, $\overline{X}_f$, is presented as follows:

$$\overline{X}_f = \frac{1}{10}\sum_{i=1}^{10} \overline{X_i} \tag{2.2}$$

- Variance
  The variance of the data set X consisting of n samples is defined as $\langle s^2 \rangle$ and given by the equation:

$$\langle s^2 \rangle = \frac{1}{n-1} \sum_{i=1}^{n} \left[(x_i - \overline{X})^2 \right] \tag{2.3}$$

- Standard deviation
  The positive square root of the variance, $\langle s^2 \rangle$, is denoted by σ and presented as follows:

$$\sigma = \sqrt{\langle s^2 \rangle} \tag{2.4}$$

- RMS (Root Mean Square)
  The root mean square of a sequence X is determined as the positive square root of the mean of the square of the input sequence. The formula used to compute the RMS value is given by the equation:

$$RMS = \sqrt{\frac{1}{n} \sum_{i=0}^{n-1} {X_i}^2} \tag{2.5}$$

However, the analysis of the signal in the time domain is generally not sufficient. To study all information, which signal contains, it is necessary to transform this signal to the frequency domain, what can be done by the Fourier Transformation described in the following section.

2.1.1.1.1 FFT method

The strongly optimized algorithm, Fast Fourier Transformation, has been chosen because of its shorter time of computation. FFT reduces the number of calculations needed for N points to $N \cdot \log_2 N$ comparing to N^2 of the DFT (Discrete Fourier Transform). Therefore, the following paragraph presents the use of FFT method. According to Fourier theory any function f(x) with period 2π ($f(x) = x + 2\pi$) can be described in terms of an infinite sum of sines and cosines, as follows:

$$f(x) = \frac{a_0}{2} + \sum_{m=1}^{\infty} (a_m cosmx + b_m sinmx) \tag{2.6}$$

Where a_0, a_m and b_m are the Fourier coefficients defined by:

$$a_m = \frac{1}{\pi}\int_{-\pi}^{\pi} f(x)cosmxdx \tag{2.7}$$

$$b_m = \frac{1}{\pi}\int_{-\pi}^{\pi} f(x)sinmxdx \tag{2.8}$$

$$a_0 = \frac{1}{\pi}\int_{-\pi}^{\pi} f(x)dx \tag{2.9}$$

The result of the FFT analysis is an array of complex numbers, amplitudes and phases, corresponding to elementary harmonic oscillations into which the signal may be decomposed. The amplitudes correspond to the power spectrum, which shows the amount of power in a given frequency band or in a given line. The frequency spectrum can be used as a tool to distinguish different regimes of periodicity, chaos and noise.
In the frame of this thesis, Fast Fourier Transform has been applied under LabView platform. It provides a complete set of tools to perform Fourier and spectral analysis.

2.1.1.1.2 Application to arc voltage

The measurement of the arc voltage signal has been carried out using a data acquisition PCI 6132 computer card piloted by Labview software, as has been presented above. This PCI 6132 card consists of 4 simultaneously sampled analog inputs limited by the level voltage of ±10 V. Therefore, to make the measurements of the arc voltage the bridge circuit has to be implemented. The resistors R_1 and R_2 are respectively 2.16 kΩ and 48.93 kΩ, what gives the value of divider equals 23.65, obtained by using the following equation:

$$U_{out} = \frac{R_1}{R_1 + R_2}U_{in} \tag{2.10}$$

The measurement of the circuit has given the value of divider equals 22.86. The difference between the calculated value of divider and the measured one is caused by the heat dissipation of the resistors, what results in differential resistances.
As has been presented above, the sampling process is crucial in the time-resolved measurements. Because of fast variations of re-arcing phenomena in the plasma torch (up to 50 μm) the sample rate of 320 kS/s during 0.2 s has been chosen. It gives a sampling frequency of 160 kHz which meets the Nyquist sampling criterion and the frequency resolution equals to approximately 5 Hz.

	A(X)	B(Y)	C(Y)	D(Y)	E(Y)	F(Y)	G(Y)	H(Y)	I(Y)	J(Y)	K(Y)	L(Y)	M(Y)
Long Name	Time	V(t)	Vh(t)	Va(t)	Vr(t)	Frequency	FFT(V)	FFT(Vh)	FFT(Va)	FFT(Vr)	Frequency filter	Fh	Fa
Units	s	V				Hz							
Comments													
Sparklines													
1	0	-4,52395	-9,08004	2,60496	1,95113	0	8,51898E-32	1,56212E-34	2,68678E-36	7,71369E-32	0	0,04282	0,00562
2	3,1E-6	-9,99507	-8,61457	2,35585	-3,73635	4,96278	0,00464	8,5493E-6	1,46703E-7	0,0042	4,96278	0,04292	0,00562
3	6,2E-6	-13,92578	-8,11813	2,04925	-7,85691	9,92556	0,01046	1,93508E-5	3,31279E-7	0,00947	9,92556	0,04301	0,00563
4	9,3E-6	-15,59899	-7,59213	1,69476	-9,70162	14,88834	0,00526	9,7783E-6	1,67012E-7	0,00476	14,88834	0,04311	0,00563
5	1,24E-5	-15,86458	-7,03887	1,30252	-10,12823	19,85112	0,01107	2,0662E-5	3,52079E-7	0,01001	19,85112	0,04321	0,00564
6	1,55E-5	-15,75834	-6,4612	0,88311	-10,18025	24,8139	0,01036	1,9432E-5	3,30345E-7	0,00937	24,8139	0,0433	0,00565
7	1,86E-5	-15,43964	-5,86225	0,44738	-10,02477	29,77668	0,0042	7,91678E-6	1,34271E-7	0,0038	29,77668	0,0434	0,00565
8	2,17E-5	-14,64287	-5,24528	0,00626	-9,40385	34,73945	0,01084	2,05124E-5	3,4708E-7	0,0098	34,73945	0,04349	0,00566
9	2,48E-5	-13,60708	-4,61377	-0,42954	-8,56376	39,70223	0,00328	6,23241E-6	1,05208E-7	0,00297	39,70223	0,04359	0,00566
10	2,79E-5	-12,70408	-3,97127	-0,84974	-7,88306	44,66501	0,00354	6,74968E-6	1,13671E-7	0,00319	44,66501	0,04369	0,00567
11	3,1E-5	-11,66828	-3,32129	-1,24465	-7,10234	49,62779	0,01817	3,48358E-5	5,85284E-7	0,01641	49,62779	0,04379	0,00568
12	3,41E-5	-10,76528	-2,66728	-1,60537	-6,49263	54,59057	0,01147	2,20857E-5	3,7019E-7	0,01036	54,59057	0,04389	0,00568
13	3,72E-5	-10,02163	-2,01258	-1,92396	-6,08509	59,55335	0,00253	4,9042E-6	8,20074E-8	0,00229	59,55335	0,04399	0,00569
14	4,03E-5	-9,17175	-1,36035	-2,19358	-5,61782	64,51613	0,00572	1,11147E-5	1,85418E-7	0,00516	64,51613	0,04408	0,00569
15	4,34E-5	-9,35766	-0,71359	-2,4086	-6,23547	69,47891	0,01215	2,37167E-5	3,94707E-7	0,01097	69,47891	0,04419	0,0057
16	4,65E-5	-10,26066	-0,07483	-2,56458	-7,62125	74,44169	0,00372	7,28773E-6	1,20998E-7	0,00335	74,44169	0,04428	0,00571
17	4,96E-5	-11,00431	0,55378	-2,65837	-8,89972	79,40447	0,02389	4,70579E-5	7,79439E-7	0,02155	79,40447	0,04439	0,00571
18	5,27E-5	-10,89807	1,17016	-2,68839	-9,37985	84,36725	0,01938	3,83571E-5	6,33805E-7	0,01749	84,36725	0,04448	0,00572
19	5,58E-5	-10,26066	1,77211	-2,65475	-9,37803	89,33003	0,00205	4,07648E-6	6,71979E-8	0,00185	89,33003	0,04459	0,00572
20	5,89E-5	-9,38422	2,35731	-2,55922	-9,1823	94,2928	0,0029	5,79446E-6	9,52886E-8	0,00262	94,2928	0,04469	0,00573
21	6,2E-5	-8,32187	2,92344	-2,40513	-8,84018	99,25558	0,02472	4,9584E-5	8,1344E-7	0,02228	99,25558	0,04479	0,00574
22	6,51E-5	-6,78145	3,46821	-2,19719	-8,05247	104,21836	0,0171	3,4466E-5	5,64064E-7	0,01542	104,21836	0,04489	0,00574
23	6,82E-5	-5,00201	3,98928	-1,94145	-7,04984	109,18114	0,00328	6,64001E-6	1,08408E-7	0,00296	109,18114	0,04499	0,00575
24	7,13E-5	-2,95698	4,48434	-1,64504	-5,79628	114,14392	0,00773	1,57267E-5	2,5614E-7	0,00697	114,14392	0,0451	0,00575
25	7,44E-5	-0,83227	4,95109	-1,31596	-4,4674	119,1067	0,02899	5,92148E-5	9,621E-7	0,02611	119,1067	0,0452	0,00576
26	7,75E-5	1,39867	5,38738	-0,96287	-3,02585	124,06948	0,01558	3,19721E-5	5,18211E-7	0,01403	124,06948	0,0453	0,00577
27	8,06E-5	3,65617	5,79118	-0,59475	-1,54025	129,03226	0,00192	3,95307E-6	6,39169E-8	0,00173	129,03226	0,04541	0,00577
28	8,37E-5	6,09958	6,16061	-0,22076	0,15973	133,99504	0,0254	5,26123E-5	8,48616E-7	0,02287	133,99504	0,04551	0,00578
29	8,68E-5	8,78203	6,49396	0,1501	2,13796	138,95782	0,02483	5,16659E-5	8,31321E-7	0,02235	138,95782	0,04561	0,00579
30	8,99E-5	11,59726	6,78968	0,50914	4,29844	143,9206	0,01589	3,32146E-5	5,3313E-7	0,0143	143,9206	0,04572	0,00579
31	9,3E-5	14,46562	7,04645	0,84826	6,5709	148,88338	0,02811	5,9015E-5	9,44938E-7	0,02528	148,88338	0,04582	0,0058
32	9,61E-5	10,42867	7,26353	1,1604	2,00474	153,84615	0,00944	1,99195E-5	3,18166E-7	0,00849	153,84615	0,04593	0,0058
33	9,92E-5	1,13308	7,44264	1,44066	-7,75023	158,80893	0,00114	2,41367E-6	3,84581E-8	0,00102	158,80893	0,04603	0,00581
34	1,02E-4	-3,22257	7,58722	1,68599	-12,49578	163,77171	0,00691	1,47196E-5	2,33958E-7	0,00622	163,77171	0,04614	0,00582
35	1,05E-4	-3,78031	7,69949	1,89332	-13,37311	168,73449	1,15E-4	2,46416E-7	3,90696E-9	1,04E-4	168,73449	0,04625	0,00582

Figure 2.3: Example of the structure of the recorded data.

The example of the data structure of the arc voltage signal, recorded at 400 A for Ar-H_2 (45-10 slm) plasma by the torch with a standard configuration of the cathode cavity: V_g = 6 cm^3, is shown in Figure 2.3. The measured and calculated results have been processed by the Origin Pro software to present the temporal evolution of the fluctuating component of the arc voltage signal $\upsilon(t)$, what is given in Figure 2.4. These variations have been obtained from the instantaneous voltage, V(t), which is considered as the sum of the mean voltage, $\overline{V}$, and of the fluctuating component, $\upsilon(t)$.

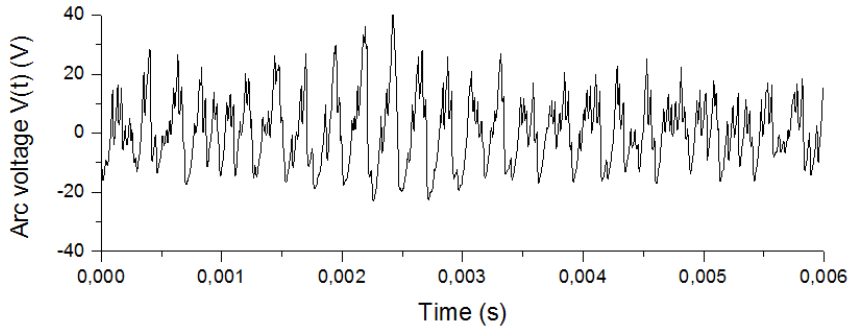

Figure 2.4: Time evolution of the fluctuating component of the arc voltage signal.

The statistical analysis of this signal, performed by Labview program, is indicated in Table 2.2.

Table 2.2: Statistical analysis of the signal presented in Figure 2.4.

$\overline{V}$ (V)	σ (V)	$\langle \upsilon^2 \rangle$ (V)	RMS (V)
62	13.1	171.7	62.5

The mean value, standard variation, variance and RMS of the signal have been calculated.

The obtained temporal evolution of the arc voltage signal shows the characteristic features related to the restrike mode but they are superimposed on more regular oscillations, pseudo sine wave with the period of about 200 μs. Therefore, to complete the analysis of the measured arc voltage Fast Fourier Transformation has been performed.
To compare computed power spectra of the signals measured under different experimental conditions, presented in the further paragraphs, each spectrum has been normalized with respect to the variance of the voltage. As has been presented above, the instantaneous voltage, V(t), is the sum of the mean voltage, $\overline{\mathrm{V}}$, and of the fluctuating component, v(t). The average squared quantities are obtained as follows:

$$\langle V^2 \rangle = \overline{V}^2 + \langle v^2 \rangle \tag{2.11}$$

where $\langle v^2 \rangle$ is the variance of the voltage, presented in Table 2.2.
The power spectrum, ϕ(f), of the voltage fluctuating component, v(t), which is the squared amplitude of its Fourier components, is then given by:

$$\int_0^{f_{max}} \phi(f)df = \langle v^2 \rangle \tag{2.12}$$

Figure 2.5 presents the computation of the voltage power spectrum of the signal given in Figure 2.4.

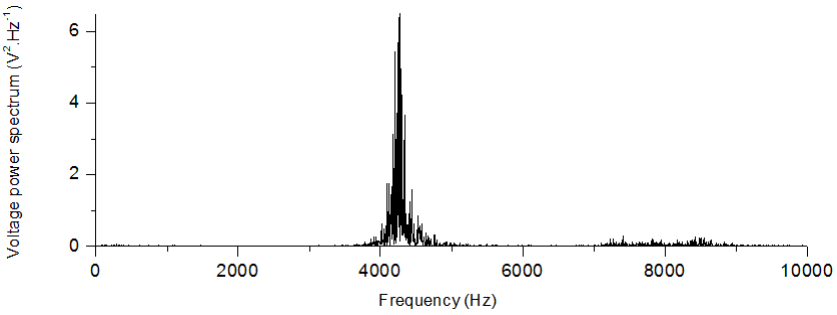

Figure 2.5: Voltage power spectrum of the arc voltage signal presented in Figure 2.4.

2.1.1.1.3 Resonance in dc plasma torch

The power spectrum, presented in Figure 2.5, highlights the presence of a sharp peak at ~4.3 kHz, what cannot correspond to mentioned in chapter 1 restrike fluctuations, which are characterized by non-reproducible spectral components. This spectral peak matches, approximately, to the reverse of the period of the above-mentioned sine wave in Figure 2.4. The obtained results suggest that in dc plasma torch is another phenomenon superimposed on the restrike mode.

One of the explanation of this phenomenon could be the existence of the acoustic wave in the nozzle in which resonance could take place, provided the length of the channel is an integer multiple of the half wavelength. However, the length of the nozzle torch should be of about 0.6 m instead of around 30 mm, given in Table 2.1. Therefore, acoustic longitudinal stationary waves cannot occur at this frequency in this nozzle channel.

In the description of the plasma instabilities presented in chapter 1 the linear dependence of the mean measured pressure on the specific enthalpy and, therefore, the mean voltage has been highlighted (see Figure 1.27). It has leaded to the idea to consider the coupling between the arc and pressure variations in the cathode cavity. These variations of the pressure can be generated by the oscillation of the plasma into the nozzle channel, what shows that the cathode cavity together with the nozzle channel can appear to be a Helmholtz resonator.
Delair *et al.* has first suggested that Helmholtz oscillations in the arc chamber can be the reason for high frequency fluctuations of the arc voltage [69]. This hypothesis has been referred to the field of combustion systems where it has been discovered that the burners behave like Helmholtz resonators [70, 71].
The Helmholtz oscillation is a very basic phenomenon studied in the framework of vibration theory. The resonator is a simple acoustic system, presented in Figure 2.21, which consists of a rigid-walled cavity of volume V, filled with air, with a neck of section S and the length L.

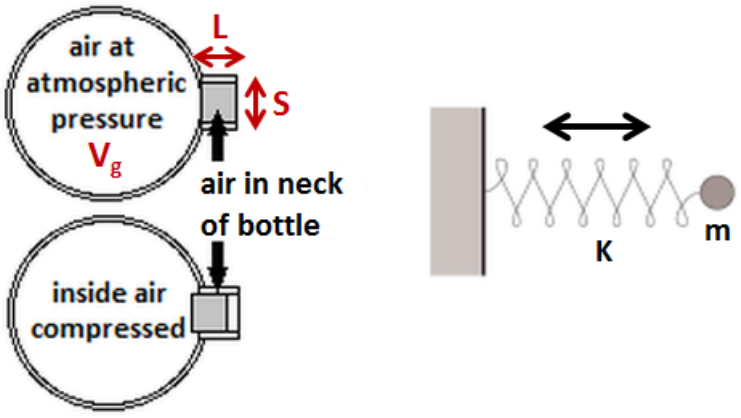

Figure 2.6: Helmholtz resonator as mass-spring system.

The air filling the system is under the atmospheric pressure. After a proper short exterior pressure excitation, the air in the neck is starting to move back and forth damping out in time. The Helmholtz resonator is commonly compared to the mass-spring system. The air filling the cavity, submitted to condensations and rarefactions, acts like a spring. The air located in the neck plays the role of an incompressible mass moving back and forth along the neck.

The mass of the air in the neck can be presented by the equation:

$$m = \rho.S.L \tag{2.13}$$

where:

ρ is the density of air.

If this mass descends a small distance x into the neck, it compresses the air in the cavity so that the air that previously occupied the volume V now has the volume: $V - S.x$. Consequently, the pressure of the air rises from atmospheric pressure, P_0, to the value: $P_0 + p$.
Assuming the oscillations to be adiabatic, the pressure change p/P_0 produced by this small volume change, ΔV, is equal to:

$$\frac{p}{P_0} = -\gamma\frac{\Delta V}{V} = -\gamma\frac{Sx}{V} \tag{2.14}$$

This mass of the air, m, is moved by the difference in pressure between the top and bottom of the neck, what can be presented by Newton law for the acceleration:

$$m\frac{d^2x}{dt^2} = F \tag{2.15}$$

assuming that F is a net force presented by F = pS and introducing m determined by Equation (2.13), it gives:

$$\frac{d^2x}{dt^2} = \frac{p.S}{\rho.S.L} = -\frac{\gamma SP_0}{\rho.V.L}x \tag{2.16}$$

It shows that restoring force is proportional to the displacement. This is the condition for simple harmonic motion, which has a frequency $1/2\pi$ times the square root of the constant of proportionality, as follows:

$$f = \frac{1}{2\pi}\sqrt{\frac{\gamma SP_0}{\rho.V.L}} \tag{2.17}$$

While determining the speed of sound in air, c, by the density, the pressure and ratio of specific heats, the resonant frequency is given by the equation:

$$f = \frac{c}{2\pi}\sqrt{\frac{S}{V.L}} \tag{2.18}$$

The cold gas in the cathode cavity, characterized by the volume V_g, presented in Figure 2.7, is analogous to the air in the cavity of the Helmholtz resonator, described above, and to the spring in the mass-spring system.

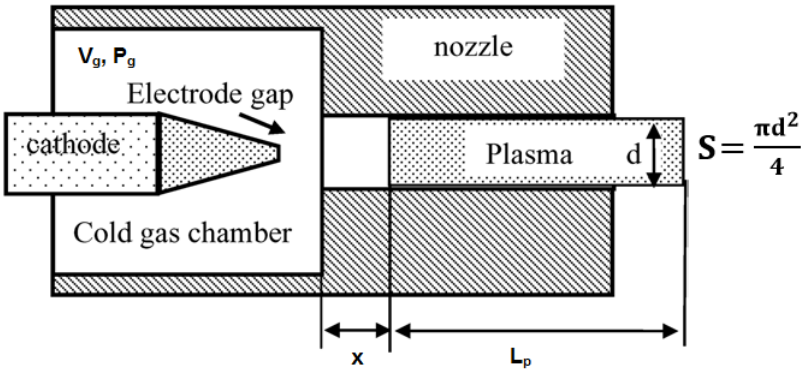

Figure 2.7: Schematic view of the plasma Helmholtz oscillations.

This cathode cavity is connected to the nozzle channel which contains the oscillating plasma (compared to the mass in the mass-spring system). The oscillating plasma induces the pressure drop due to the friction resistance and turbulence, which added to the viscous effects in the channel, is a source of non-reversible phenomena. Then, the pressure perturbation in the cathode cavity is given by the equation:

$$\frac{d^2p}{dt^2} + \frac{\omega_H}{Q}\frac{dp}{dt} + {\omega_H}^2 p = {\omega_H}^2 p_{ext} \tag{2.19}$$

where:

p_{ext} is the excitation source of the resonator coupled with the arc voltage,
Q the quality factor due to dissipative effects.

This Q factor is linked to the band pass of the resonator, Δf, and to the damping factor, ξ, as follows:

$$Q = \frac{f_H}{\Delta f} = \frac{1}{2\xi} \tag{2.20}$$

By applying similar assumptions to the plasma mass as has been presented above, for a Helmholtz resonator, a Helmholtz frequency of plasma mass motion in the torch nozzle can be defined as:

$$f_H = \frac{1}{2\pi}\sqrt{\frac{\gamma_g P_g}{\rho_p}}\sqrt{\frac{S}{L_p V_g}} \tag{2.21}$$

where:

γ_g is the isentropic coefficient of the cold gas,
P_g the mean pressure in the cathode cavity,
ρ_p the plasma density,
S the cross section area of the torch nozzle, presented in Figure 2.7,
L_p the length of the nozzle channel,
V_g the volume of the cathode cavity.

The equation (2.21) highlights the dependence of the Helmholtz mode on the thermophysical properties, γ_g and ρ_p, related, respectively, to the cold gas and to the plasma, the torch configuration, $\sqrt{S/L_p.V_g}$ and the pressure in the cathode cavity, what is the function of the working conditions and of the thermodynamic properties of the gas.

Consequently, the investigation of Helmholtz mode of plasma oscillations requires the simultaneous measurements of the arc voltage and the pressure inside the cathode cavity. The time-resolved total pressure has been measured using a piezoresistive sensor ENDEVCO 8510C (Meggitt's Endevco, Irvine, USA). It is a miniature and high sensitivity piezoresistive transducer for measuring dynamic pressure (in ranges from 15 to 100 psi). A small size, 4 mm in diameter, enables to mount this sensor in the cathode cavity of the torch. The simultaneous measurements of the arc voltage and the pressure signals have been performed using a data acquisition PCI 6132 computer card piloted by Labview software, what has been highlighted in the previous paragraphs.

2.2 Investigation of the plasma instabilities

The theoretical model of Helmholtz mode has highlighted the dependencies of Helmholtz fluctuations on the geometrical parameters of the torch and the thermophysical properties related to the cold gas and to the plasma. Therefore, the purpose of the presented studies is to confirm this model by the experimental measurements. The influence of different operating conditions will be examined by measuring the arc voltage signals and the pressure inside the cathode cavity.
Moreover, the previous work of the laboratory has highlighted the existence of other fluctuation modes due to acoustic waves propagation and reflection inside the torch [72, 73]. These modes, so-called acoustic modes, occur at higher frequencies, presented as a divergent peak at ~8.5 kHz in the voltage power spectrum in Figure 2.5. Therefore, the following sections will give the investigation results of the Helmholtz and acoustic modes. Moreover, the arc voltage signal presents more randomly distributed short events which correspond to the restrike mode, what will be also studied in this work.
To examine the Helmholtz, acoustic and restrike modes of the plasma instabilities, the signals of these modes have to be isolated from the measured arc voltage and pressure by applying the filtering methods, what is described in the following section.

2.2.1 Filtering method

The fluctuating component, υ(t), obtained from the measured arc voltage signal, V(t), where υ(t) = V(t) - $\overline{\text{V}}$, can be presented as the sum of the instability modes of plasma jet: Helmholtz (H), restrike (R) or acoustics (a), as follows:

$$\upsilon(t) = \upsilon_H(t) + \upsilon_R(t) + \upsilon_a(t) \tag{2.22}$$

The time-resolved measurement of the pressure can be also predicted as the superposition of the modes of the plasma fluctuations. The signal of the arc voltage or the pressure which contains several components can be written as:

$$s(t) = \sum_i s_i(t) \tag{2.23}$$

where the subscript, i, is associated with the modes of the instability.
To observe the influence of these modes on the operating conditions they have been isolated from the signal by using numerical Wiener filter programmed under LabView platform. The purpose is to separate each component, s_i(t), by using a Wiener filter, F_i(f), which is obtained by a minimization method (minimization of the Euclidean distance between the ideal s_i(t) function and the one obtained by filtering, S_i(f)) as follows:

$$\frac{\partial}{\partial F_i} = \left\{ \int \parallel s_i(t) - FT^{-1}\{F_i(f) \times S(f)\} \parallel^2 dt \right\} = 0 \tag{2.24}$$

where:

TF^{-1} is the reciprocal Fourier transform,
S(f) the Fourier transform of the recorded signal, s(t), defined as S(f) = FT{s(t)} where $S(f) = \sum_i S_i(f)$.

By applying the Plancherel-Parseval theorem, the above equation can be written as:

$$\frac{\partial}{\partial F_i} = \left\{ \int_0^{f_{max}} \parallel S_i(f) - \{F_i(f) \times S(f)\} \parallel^2 dt \right\} = 0 \tag{2.25}$$

what gives the following formula:

$$\int_0^{f_{max}} \frac{\partial}{\partial F_i} \parallel S_i - F_i \times S \parallel^2 df = \int_0^{f_{max}} \{2F_i \times SS^* - (SS_i^* + S^*S_i)\} df = 0 \tag{2.26}$$

where:

$*$ stands for the complex conjugate.

The expansion of S gives cross products, such as $S_i S_j^*$. Assuming that the instability modes are uncorrelated either because the frequency domains of i and j components are disconnected or by phase mixing if the restrike mode is implied, the optimum Wiener filter, F_i, is given by:

$$F_i(f) = \frac{\Phi_{ii}}{\Phi_{HH} + \Phi_{RR} + \Phi_{aa}} \tag{2.27}$$

where Φ_{HH} and Φ_{aa} are obtained by fitting a Lorentzian function to each peak of the recorded spectrum, as follows:

$$\Phi_{ii}(f) = \frac{A_i}{1 + 4{Q_i}^2 (f - f_i)^2} \tag{2.28}$$

Figure 2.8 presents the filters F_H and F_a determined from the arc voltage spectrum, from Figure 2.5, recorded for a plasma torch operated at 400 A and Ar-H_2 (45-10 slm) gas mixture, what was indicated in Figure 2.4. Figure 2.8 highlights that the calculated filter is a real function of frequency and does not produce phase shifts.

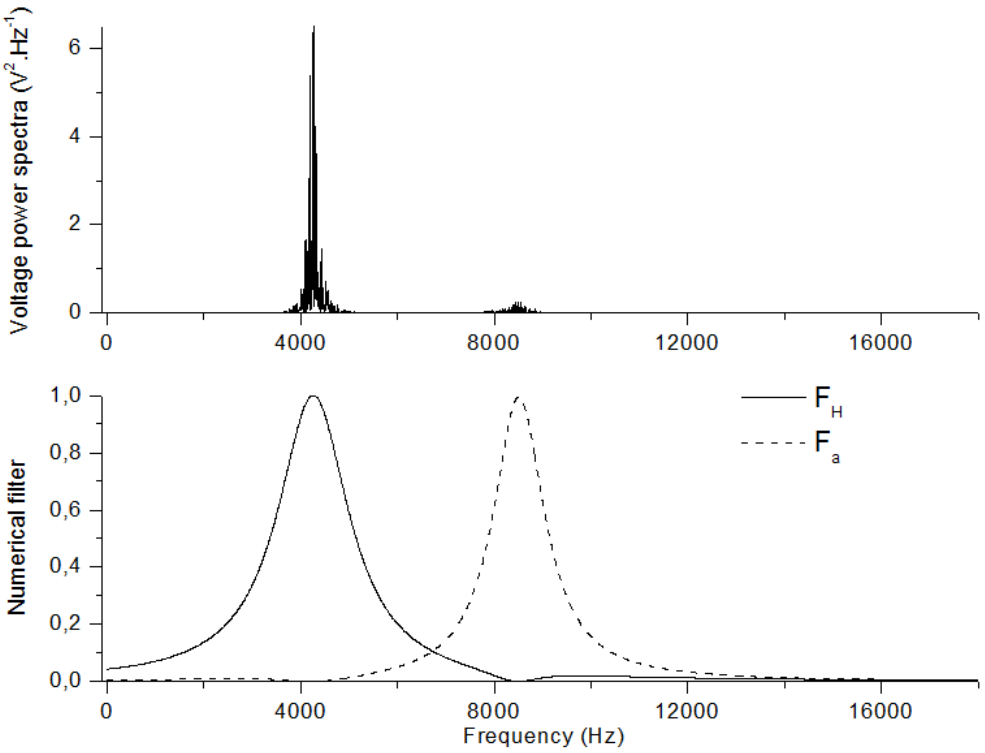

Figure 2.8: Calculated filters F_H and F_a applied to the power spectrum, presented in Figure 2.5, of the arc voltage generated for the conditions from Figure 2.4.

The determination of the filters: F_H and F_a allows obtaining Helmholtz and acoustic modes components by the following equation:

$$s_i(t) = FT^{-1}\{F_i(f) \times S(f)\} \tag{2.29}$$

Then, the restrike component can be deduced as follows:

$$s_R(t) = s(t) - [s_H(t) + s_a(t)] \tag{2.30}$$

Figure 2.9 presents the example of the filtering from a raw arc voltage signal its components: the restrike, Helmholtz and acoustic modes of instabilities. It shows that the Helmholtz component has the most important contribution to the arc voltage together with the restrike mode. A modulation of the signal envelopes in Helmholtz and acoustic components is observed (beating phenomena).

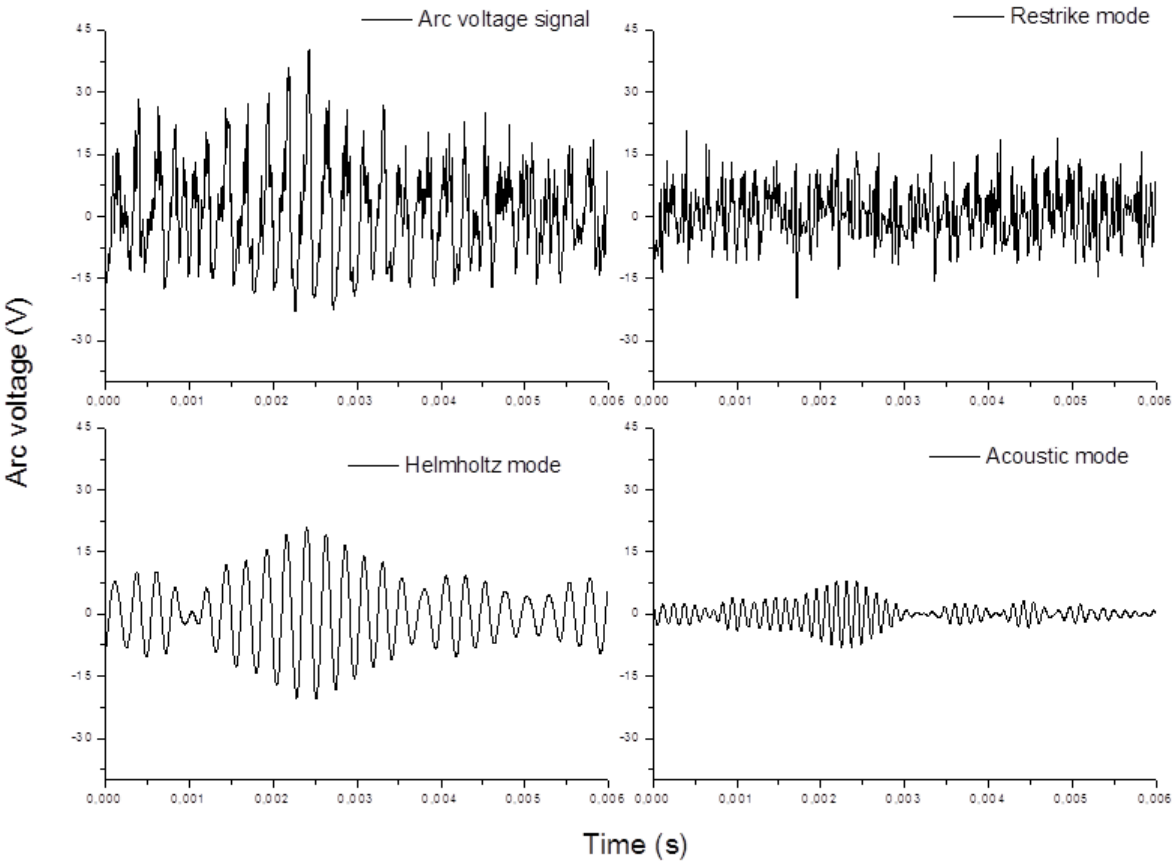

Figure 2.9: Raw arc voltage signal, from Figure 2.4, and its filtered components: Helmholtz, restrike and acoustic.

Similar behavior has been observed for the fluctuating component of pressure.

2.2.2 Helmholtz and acoustic modes

The following section will highlight experimentally the dependence of the Helmholtz and acoustic modes on the geometrical parameters of the torch: the volume of the cavity and the position of the cathode. Moreover, the influence of the composition of plasma forming gases will be shown.

2.2.2.1 Configuration of the cathode cavity

This paragraph gives the investigation results of the effect of different configurations of the cathode cavity on the Helmholtz and acoustic modes. By removing the injection ring, Figure 2.10 (b), and using the specially machined cathode cavity, 2.10 (c), three different configurations have been obtained characterized by the volumes: (a) V_g = 12.5 cm^3, (b) V_g = 8.7 cm^3 and (c) V_g = 6 cm^3.

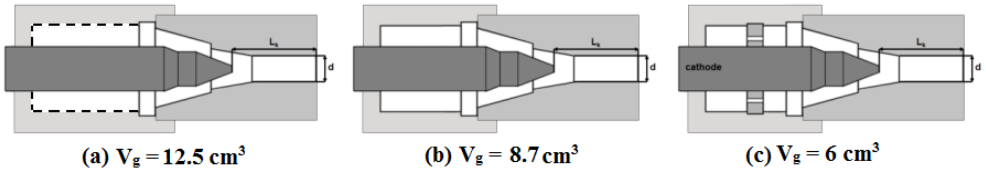

Figure 2.10: Configurations of the cathode cavity.

Figures 2.11 and 2.12 present the voltage and pressure power spectra of Helmholtz (H) and acoustic (A) components, filtered and computed from the arc voltage and pressure signals. They have been recorded for each configuration of the cathode cavity, for the same operating conditions: L_k = 30 mm, I = 500 A, Ar-H_2 (45-10 slm).

The results presented in Figures 2.11 and 2.12 show a very good matching between the Helmholtz and acoustic modes of the voltage and pressure. These results confirm the coupling between the pressure in the cathode cavity and the arc voltage, what proves that the main plasma oscillations follow the Helmholtz resonator. To analyze the evaluation of Helmholtz and acoustic modes their parameters have been established from the power spectra presented in Figures 2.11 and 2.12 and summarized in Table 2.3.
The standard deviation, defined as follows: $\sigma_i = \sqrt{\langle s_i{}^2 \rangle}$, where s_i are the signals of voltage or pressure associated with the Helmholtz, acoustic or restrike modes, has been calculated from the filtered spectra by LabView program. The Q factor has been established from Equation (2.20), as follows: $Q = f_i/\Delta f$, where Δf has been measured as the full-width at half-maximum of the Helmholtz or acoustic modes line in voltage and pressure power spectra.

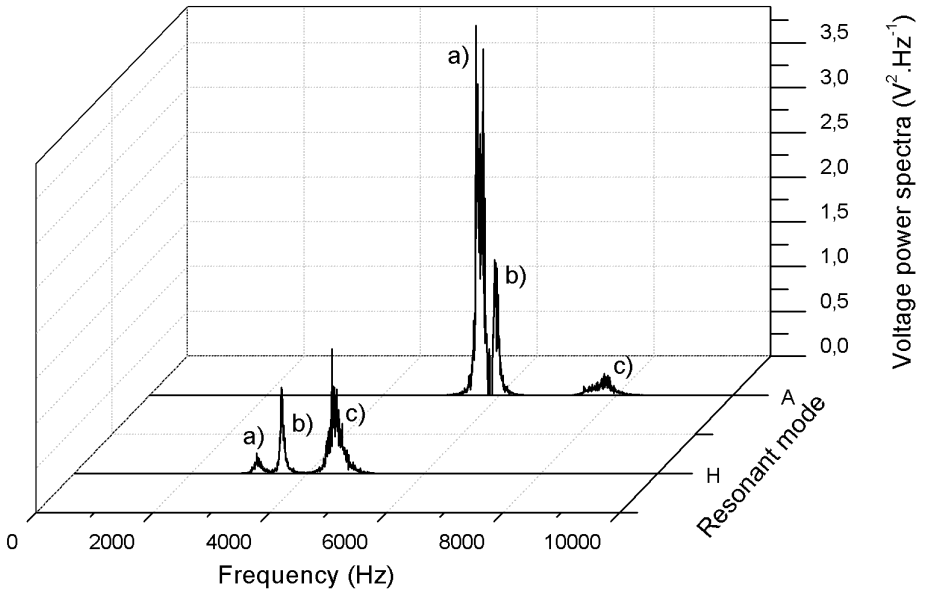

Figure 2.11: Voltage power spectra of filtered voltage fluctuations of H-Helmholtz and A-acoustic modes for: (a) V_g = 12.5 cm^3, (b) V_g = 8.7 cm^3 and (c) V_g = 6 cm^3. Operating parameters: L_k = 30 mm, I = 500 A, Ar-H_2 (45-10 slm) [74].

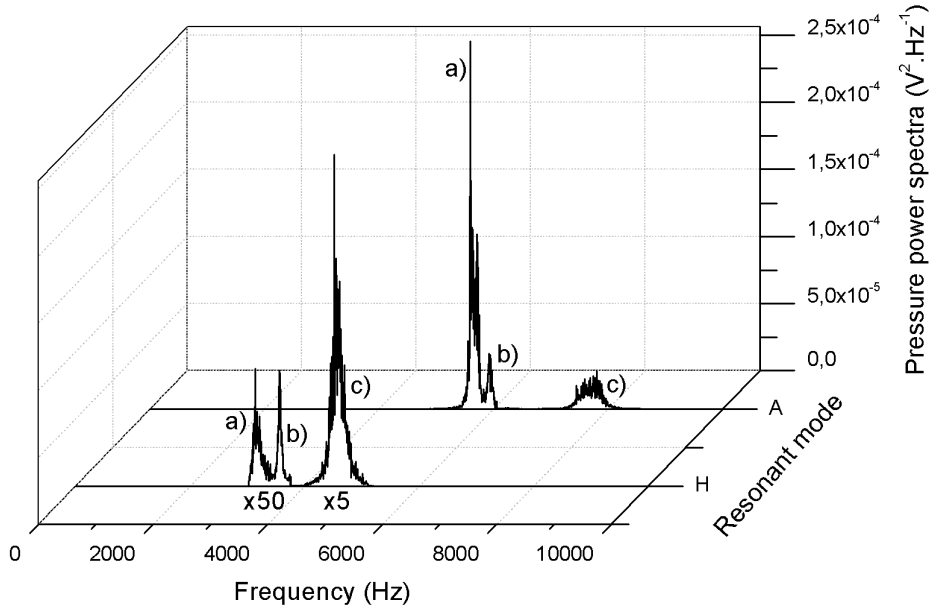

Figure 2.12: Pressure power spectra of filtered arc fluctuations of H-Helmholtz and A-acoustic modes for: (a) V_g = 12.5 cm^3, (b) V_g = 8.7 cm^3 and (c) V_g = 6 cm^3 [74].

Table 2.3: The frequency, standard deviation (σ) and Q factor of voltage and pressure power spectra presented in Figure 2.11 and 2.12, where: (a) V_g = 12.5 cm^3, (b) V_g = 8.7 cm^3 and (c) V_g = 6 cm^3.

		Arc voltage			Pressure		
		f (Hz)	σ (V)	Q	f (Hz)	σ (mbar)	Q
Helmholtz mode	(a)	3100	3.3	19	3170	3	14.5
	(b)	3600	5.5	30	3550	6	32
	(c)	4500	9	30.5	4500	53	30.5
Acoustic mode	(a)	5700	13.4	36.5	5700	90	35.5
	(b)	5950	8	43	5950	40	43
	(c)	7850	5	17	7800	56	17

The values of Helmholtz frequency of the voltage and pressure power spectra, given in Table 2.3, highlight the shift of f_H peaks to lower values due to the increase of the cathode cavity volume, e.g. from 4500 Hz obtained for the case (c) to 3100 Hz for (a). It has to be mentioned that the frequency peaks in the pressure power spectra have similar values. By following the theoretical model for Helmholtz mode, given by Equation (2.21), the modification of f_H in the function of the cathode cavity configuration can be presented as follows:

$$\left(\frac{f_1}{f_2}\right)^2 = \frac{V_2}{V_1} \tag{2.31}$$

where the subscripts 1 and 2 stands for the different cases: (a), (b) and (c) given in Table 2.3.

The calculations presented in Table 2.4 highlight a good agreement between the experimental results and the model of Helmholtz mode described in the previous section.

Table 2.4: Calculations of the Helmholtz frequency modifications due to different configurations of cathode cavity.

		Ar-H_2 (45-10 slm)			Ar-N_2 (40-6 slm)	Ar-N_2 (40-16 slm)
cavities		(a)/(b)	(b)/(c)	(a)/(c)	(a)/(c)	(a)/(c)
$(f_1/f_2)^2$	V	1.35	1.55	2.1	1.7	1.6
	P	1.25	1.6	2.02	1.7	1.6
(V_2/V_1)		1.44	1.45	2.05	2.05	2.05

The computed standard deviations of Helmholtz and acoustic modes show that with the increase of the volume of the cathode cavity, not only the Helmholtz frequencies are shifted to lower values but also a major part of the signal power turns to acoustic modes. This phenomenon is more obviously presented in Figure 2.13.

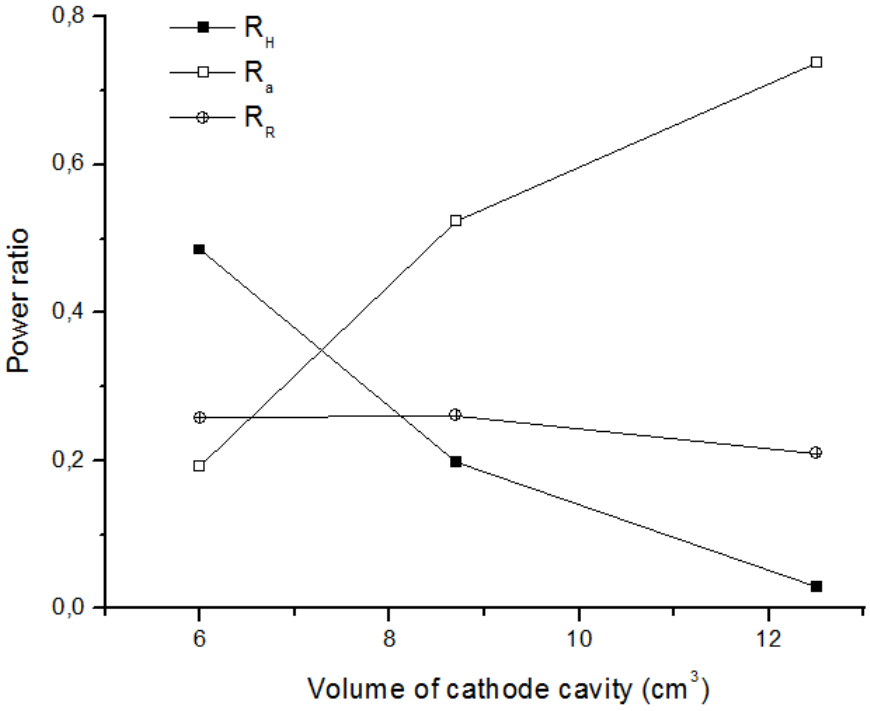

Figure 2.13: Influence of the volume of cathode cavity (cases: (a), (b), (c)) on power ratio for voltage components: H-Helmholtz, a-acoustic and R-restrike.

The power ratio, R_i, for each mode has been calculated as follows: $R_i = \sigma_i{}^2/\sigma^2$. It characterizes the power contained in each mode in relation to the raw arc voltage signal. These dimensionless power ratios have been plotted as a function of the volume of cathode cavity. For the case (c), where V_g = 12.5 cm^3, most of fluctuating power is contained in the acoustic mode oppositely to the case (a).
Moreover, the Q factors of Helmholtz resonance for the arc voltage also decrease from 30.5 to 19 when V_g varies from 6 to 12.5 cm^3. This indicates that the Helmholtz resonance energy is transferred to acoustic modes.
The presented results lead to the assumption of the model for the acoustic resonances in the conventional torch. The cathode cavity can be assumed to be of cylindrical geometry and have an annular tube shape with the length: L = 38 mm, the inner radius a = 7 mm and the outer diameter b = 10.5 mm. Defining the acoustic pressure, p, as follows: $p(\overrightarrow{r}, t) = p(\overrightarrow{r})\exp(-j\omega t)$, the acoustic modes in the cathode cavity can be determined from the solution of the homogeneous Helmholtz equation for an ideal gas obtained from the acoustic propagation equation, i.e. $\Delta p(\overrightarrow{r}, t) + k^2 p(\overrightarrow{r}, t) = 0$, where k is the wave number linked to the speed of sound, a_g, as follows: $k.a_g = 2\pi f$. The obtained resonance modes are due to a combination of the axial modes and those of radial and azimuthal modes, defined as: $k^2 = {k_r}^2 + {k_z}^2$. The cathode cavity is assumed to be an annular tube which is closed at the injection ring and supposed to be opened at the cathode tip. It can

be shown that the acoustic pressure can be written as:

$$p(r,\theta,z) = (AJ_n(k_r r) + BY_n(k_r r))cos(n\theta)cos\Big(\frac{\ell\pi}{2L}z\Big) \tag{2.32}$$

where:

r, θ, z	are the cylindrical coordinates,
J_n, Y_n	the Bessel's functions, respectively, of first and second kind of nth order,
ℓ	the integer number,
A, B	constant numbers,
L	the cathode axial length.

Since the r-component of acoustic velocity is zero at r = a and r = b, what gives $\partial p(r = a \text{ and } b, \theta, z)/\partial r = 0$, the resonance modes are obtained from the solution of the following relationship:

$$J_n'(K_r)Y_n'(\lambda K_r) - J_n'(\lambda K_r).Y_n'(K_r) \tag{2.33}$$

where:
$K_r = ak_r$,
$\lambda = b/a$,
the symbol $'$ stands for the derivation.
The resonance frequencies are: $f_{nm} = a_g K_{nm}/2\pi a$, where $K_r = K_{nm}$ are the solutions of equation (2.33), in which m gives the mth roots of equation. The resulting resonance modes have frequencies defined by:

$$f_0 = ({f_{nm}}^2 + {f_\ell}^2)^{0.5} \tag{2.34}$$

where f_ℓ corresponds to acoustic longitudinal modes and is defined as follows: $f_\ell = \ell a_g/4L$. The calculation of modes shows that most of them have frequencies above 10 kHz except the mode (n, m , ℓ) = (1, 1, 1), which defines:
the first longitudinal mode $f_\ell = 2368$ Hz and $f_{11} = 6589$ Hz, what gives the frequency $f_0 = 7000$ Hz. This value shows a good agreement of presented model with the acoustic mode frequency obtained in the power spectra presented in Figures 2.14 and 2.15. Moreover, when the volume of the cathode cavity, V_g, increases, L presented in the model (2.32) increases, what gives the decrease of the acoustic frequency. The experimental results, listed in Table 2.3 and 2.5, show the same dependency.

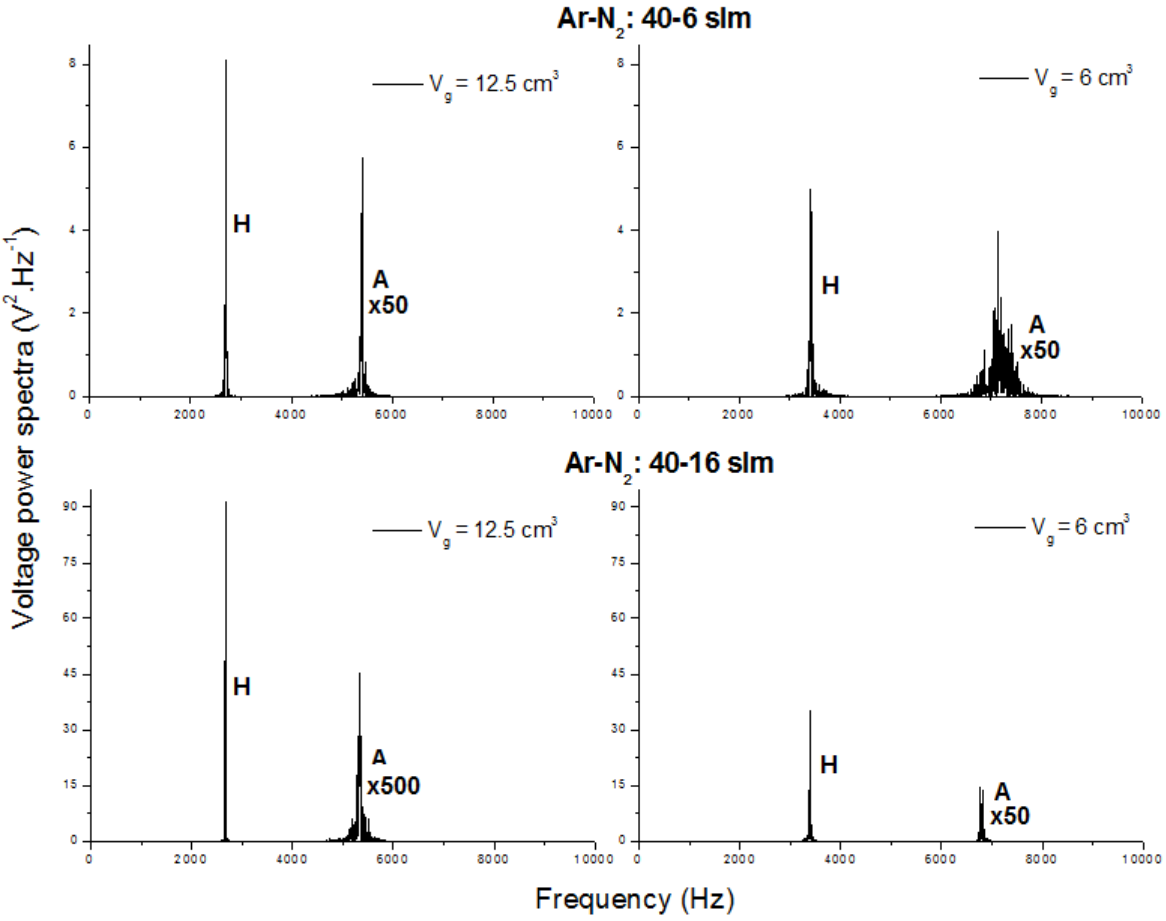

Figure 2.14: Voltage power spectra of filtered voltage fluctuations of H-Helmholtz and A-acoustic modes obtained for two configurations of cathode cavity: (a) V_g = 12.5 cm^3, (c) V_g = 6 cm^3 and for the Ar-N_2 compositions: 40-6 and 40-16 slm.

The influence of the configurations of the cathode cavity on the resonance modes has been also examined for the Ar-N_2 plasma forming gases mixtures: 40-6 and 40-16 slm. The arc voltage and pressure signals have been obtained for two configurations of the cathode cavity: (a) V_g = 12.5 cm^3 and (c) V_g = 6 cm^3 at 500 A. Figures 2.14 and 2.15 present the arc voltage and pressure power spectra computed for the signals recorded for Ar-N_2: 40-6 and 40-16 slm. The values of Helmholtz frequency, defined from the power spectra and given in Table 2.5, highlight the shift of f_H peaks to lower values, as has been expected from the model for Helmholtz mode, (2.21).

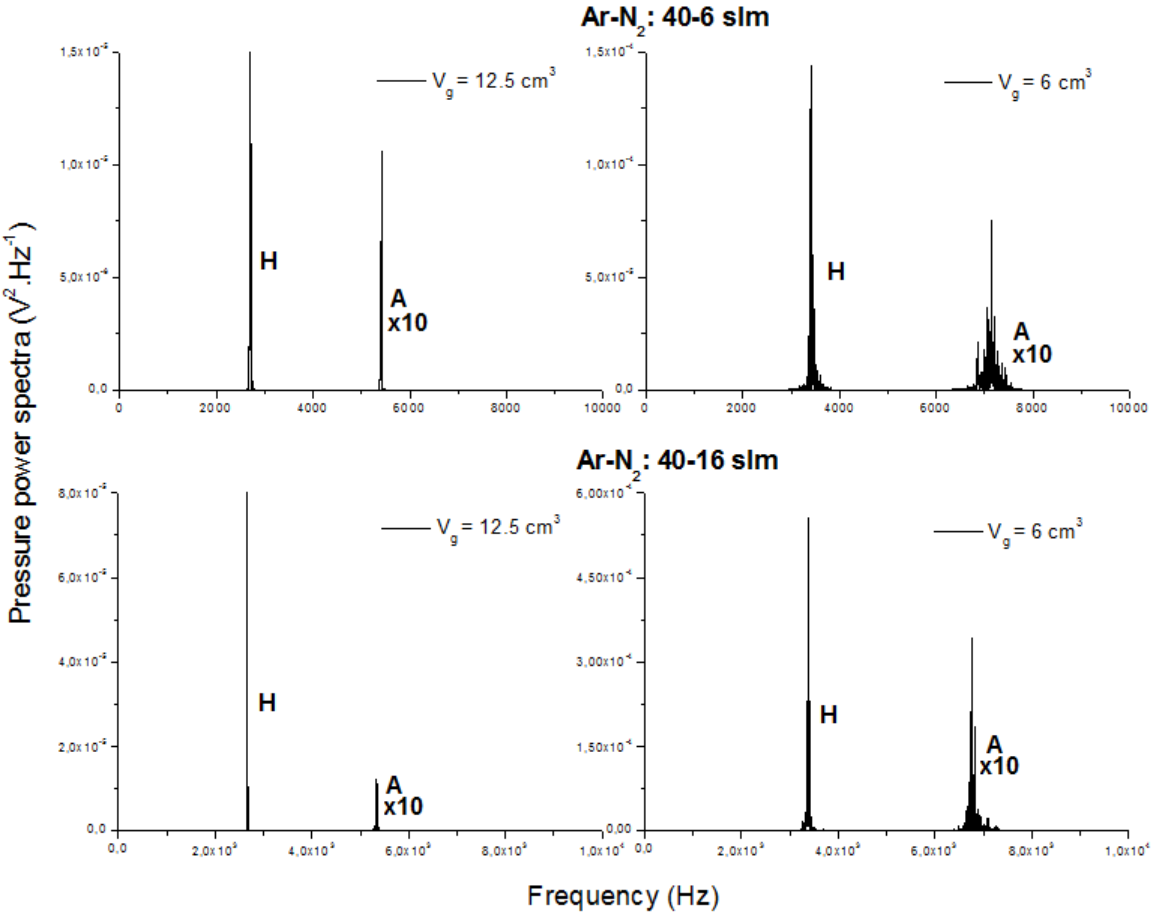

Figure 2.15: Pressure power spectra of filtered arc fluctuations of H-Helmholtz and A-acoustic modes for: (a) V_g = 12.5 cm^3 and (c) V_g = 6 cm^3.

However, the significant difference between f_H obtained for the Ar-N_2 plasma forming gases and f_H computed for Ar-H_2 has been observed, e.g. for the same configuration of cathode cavity: V_g = 6 cm^3 and the arc current = 400 A, the Helmholtz frequency, f_H, equals 3450 Hz compared to 4450 Hz of the signal measured for Ar-H_2.
Moreover, the calculated standard deviations of Helmholtz and acoustic modes show notable differences in comparison to the results obtained for the same configurations of the cathode cavity for Ar-H_2. While the volume V_g increases, particularly in the case of Ar-N_2 (40-16 slm), the Helmholtz mode of the instabilities seems to dominate, what is more clearly presented in Figure 2.16.

The power ratios for the Helmholtz, R_H, and acoustic modes, R_a, have been calculated from the filtered voltage power spectra and plotted as a function of the volume of cathode cavity. To compare the results obtained for Ar-N_2: 40-6 and 40-16 slm, the power ratios computed from signal for Ar-H_2: 45-10 slm have been indicated. All signals have been measured at the arc current of 400 A and for the configuration of cathode cavity: (a) V_g = 12.5 cm^3 and (c) V_g = 6 cm^3.

Table 2.5: The frequency, standard deviation (σ) and Q factor of voltage and pressure power spectra presented in Figure 2.14 and 2.15, for: (a) V_g = 12.5 cm^3 and (c) V_g = 6 cm^3.

		Arc voltage			Pressure		
		f (Hz)	σ (V)	Q	f (Hz)	σ (mbar)	Q
Ar-N_2 (40-6 slm)							
Helmholtz mode	(a)	2700	7.5	55	2700	11	55
	(c)	3450	9	90	3450	50	91
Acoustic mode	(a)	4650	13.4	9	4300	6	7
	(c)	7150	1.5	14	7150	19	20
Ar-N_2 (40-16 slm)							
Helmholtz mode	(a)	2700	16.5	90	2700	15	85
	(c)	3400	17	97	3400	70	97
Acoustic mode	(a)	4700	0.5	7	4300	3	5
	(c)	6800	2.5	33	6800	30	41

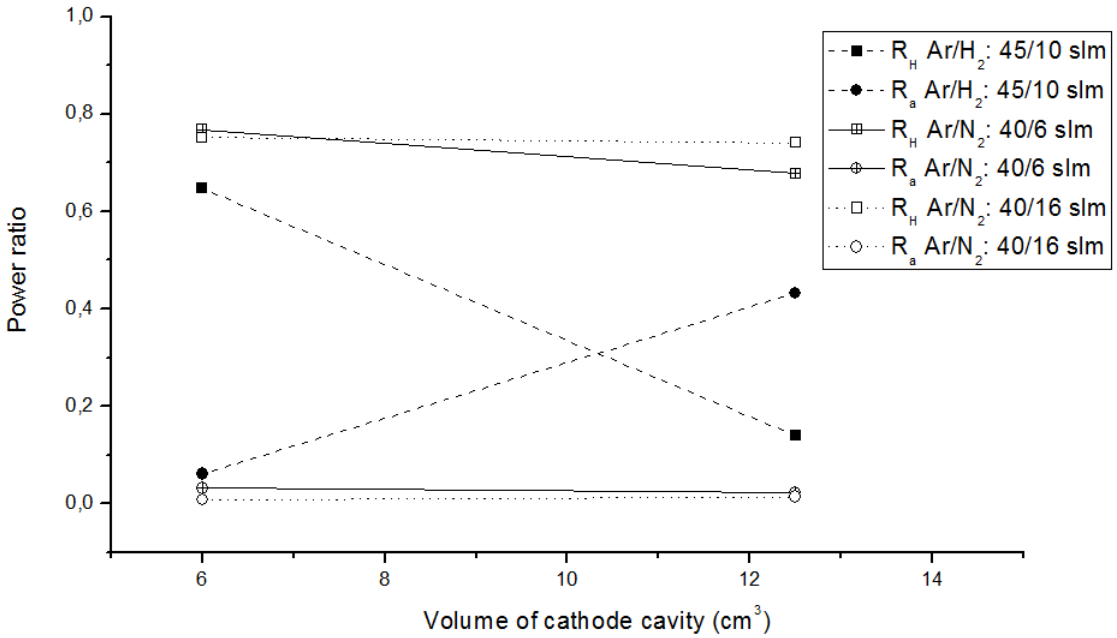

Figure 2.16: Influence of the volume of cathode cavity, for the cases: (a), (c), on power ratio for voltage components: H-Helmholtz and a-acoustic, obtained for Ar-N_2: 40-6 and 40-16 slm . To compare: the results of the power ratio computed from signal for Ar-H_2: 45-10 slm.

The obtained results show that in the case of Ar-N_2 most of fluctuating power is contained in the Helmholtz mode for both volumes V_g, what presents the different behavior than in the case of the signals obtained for Ar-H_2. This phenomenon will be more studied in the following paragraph.

2.2.2.2 Composition of plasma forming gases

In the previous studies performed in the laboratory the measurements of the arc voltage and pressure signals, obtained for argon-hydrogen mixtures as plasma forming gases, have been highlighted. The experiments have been carried out using the same home-made plasma torch, presenting a similar configuration as the commercial Sultzer Metco F4 gun. The arc voltage and pressure in the cathode cavity have been obtained at 600 A, for the constant argon flow rate at 45 slm and the hydrogen flow rate varying between 2 and 10 slm.

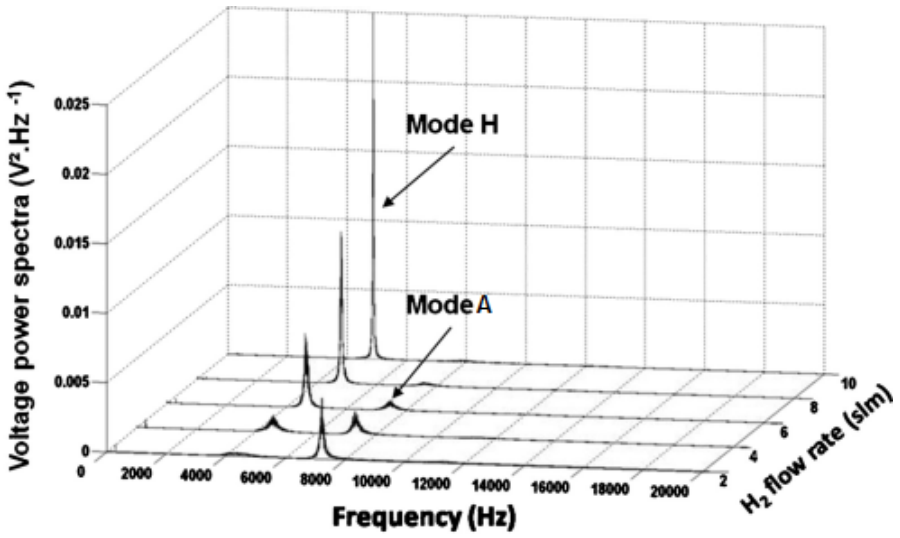

Figure 2.17: Power spectra of arc voltage calculated from signals generated at 600 A for an Ar-H_2 plasma. The mass flow rate of hydrogen varies between 2 and 10 slm [72].

The voltage power spectra, presented in Figure 2.17, show that the chemical composition of plasma forming gases strongly influences the Helmholtz resonance, especially when hydrogen content is increased in binary mixture such as Ar-H_2. Moreover, the hydrogen flow rate needs to reach a certain threshold, about 5 slm, to sustain Helmholtz oscillations. In the following paragraph, the results of the use of Ar-H_2 and Ar-N_2 as the plasma forming gases is highlighted. The results have been obtained for the following gas compositions:

- Ar-H_2 (45-5 slm)
- Ar-H_2 (45-10 slm)
- Ar-N_2 (40-6 slm)
- Ar-N_2 (40-16 slm)

The measurements of the arc voltage and pressure in the cathode cavity have been obtained at 400 A for a standard configuration of cathode cavity: case (a) $V_g = 6$ cm^3 and for the distance between cathode tip and the nozzle exit: $L_k = 30$ mm.

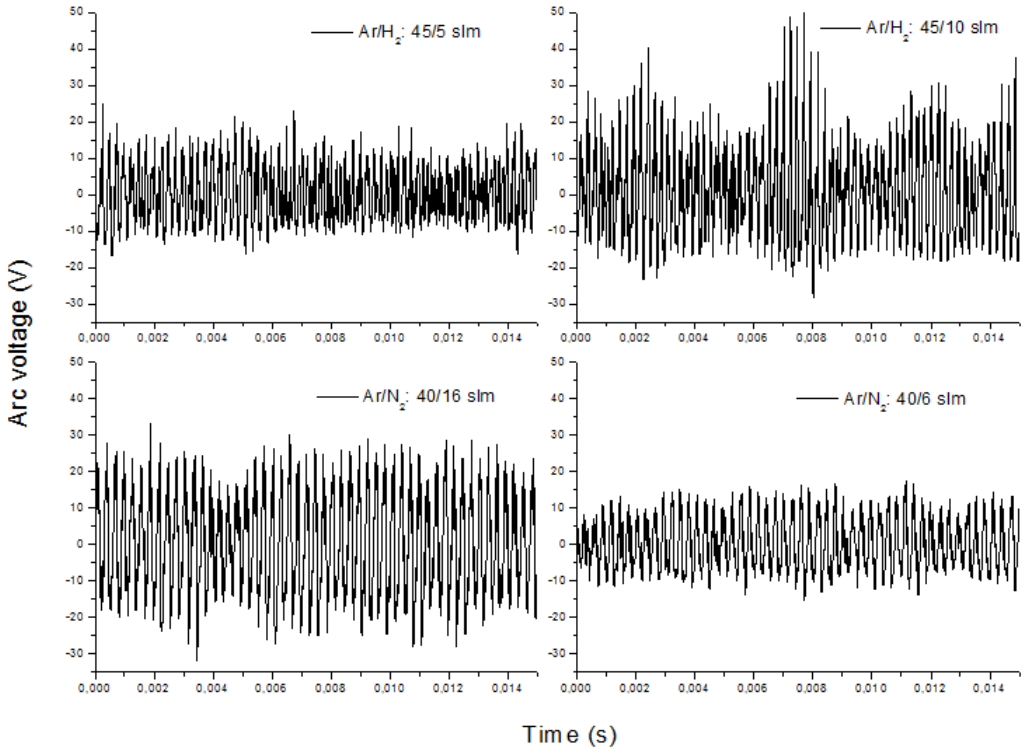

Figure 2.18: Temporal evolution of the fluctuating components of the arc voltage for argon-nitrogen and argon-hydrogen plasma.

Figure 2.18 depicts time-resolved fluctuating components of the arc voltage measured for argon-nitrogen and argon-hydrogen plasma. The calculations of the mean voltage, presented in Table 2.6, show the similar values for Ar-H_2 (45-5 slm) and Ar-N_2 (40-6 slm)- around 50 V and Ar-H_2 (45-10 slm), Ar-N_2 (40-16 slm)- around 60 V. The results obtained for Ar-H_2 mixtures have verified the experiments presented at the beginning of this paragraph, where the increase of the hydrogen content has strongly influenced the Helmholtz resonance. The voltage and pressure power spectra of the signals, in Figure 2.19 and 2.20, exhibit the same dependence. The computed standard deviations of voltage and pressure increase from 8.5 to 14.5 V and 47 to 65 mbar, what shows that a major part of signal turns to Helmholtz mode while the content of H_2 increases.

Comparing the oscillations patterns of the arc voltage obtained with an Ar-H_2 (45-10 slm) mixture to the signals measured for argon-nitrogen plasma, a significant beating component producing successive groups of peaks of high and low amplitudes is exhibited in the case of Ar-H_2 mixture.

Table 2.6: Statistical analysis of the arc voltage signals presented in Figure 2.18.

	Ar-H_2 (45-5 slm)	Ar-H_2 (45-10 slm)	Ar-N_2 (40-6 slm)	Ar-N_2 (40-16 slm)
$\overline{V}$ (V)	52	62	47	61
σ (V)	8	13	7	14
$\langle v^2 \rangle$ (V)	63	172	54	186
RMS (V)	53	63	47	62

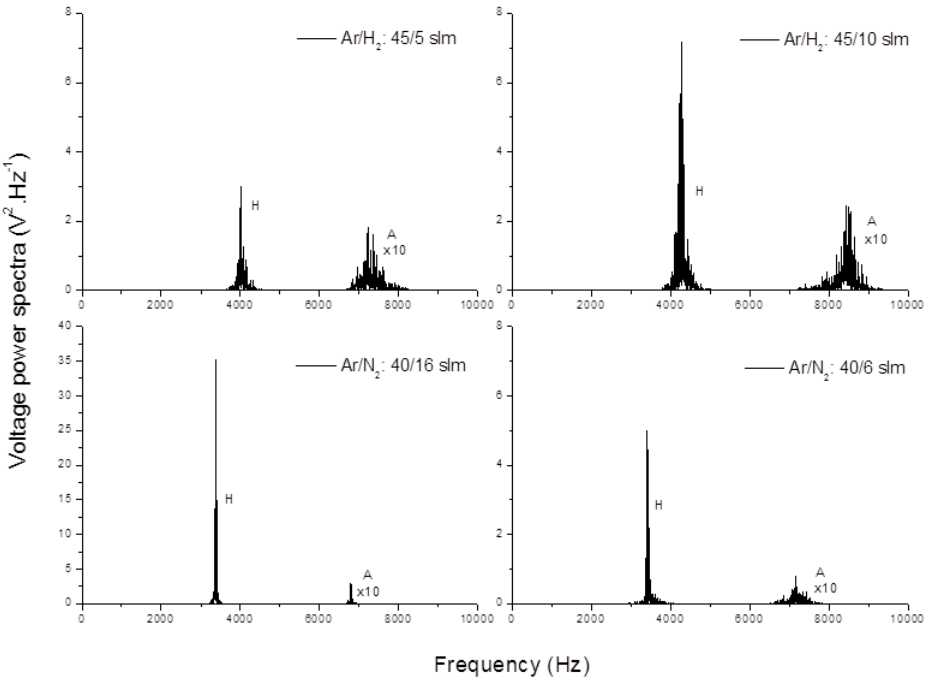

Figure 2.19: Voltage power spectra of Helmholtz and acoustic modes obtained by the filtering of the arc voltage signals presented in Figure 2.18.

The analysis of the voltage power spectra obtained with Ar-N_2 mixtures, shown in Figure 2.19, and the data given in Table 2.7 highlight that the arc voltage signals contain Helmholtz resonance without any acoustic mode influence.

Therefore, the beating phenomenon found in the temporal evolution of the fluctuating component of the voltage signal measured for Ar-H_2 (45-10 slm) mixture can be ascribed to a coupling between Helmholtz and acoustics modes.
The results shown in the previous paragraph and presented in the power spectra calculated from the arc voltage (Figure 2.19) and the pressure (Figure 2.20) signals highlight the shift of the Helmholtz frequency peaks towards the lower values for argon-nitrogen plasma. The frequency equals 3.4 kHz for Ar-N_2 (40-16 slm) plasma and 4.45 kHz for Ar-H_2 (45-10 slm). Analysing the model for Helmholtz frequency given in (2.21) this frequency drop is due to the following parameters of Ar-N_2 plasma: lower isentropic coefficient, γ, and higher density, ρ, compared to Ar-H_2 plasma.

Table 2.7: The frequency, standard deviation (σ) and Q factor of voltage and pressure power spectra, presented in Figure 2.19 and 2.20, for Ar-H_2 (45-10 slm) and Ar-N_2 mixtures.

		Arc voltage			Pressure		
		f (Hz)	σ (V)	Q	f (Hz)	σ (mbar)	Q
Ar-H_2 (45-10 slm)	H mode	4450	14	30.5	4300	72	30
	A mode	7850	3.5	17	7500	35	17.5
Ar-N_2 (40-6 slm)	H mode	3450	9	90	3450	49	91
	A mode	7150	1.5	14	7150	19	20
Ar-N_2 (40-16 slm)	H mode	3400	17	97	3400	68	97
	A mode	6800	2.5	33	6800	30	41

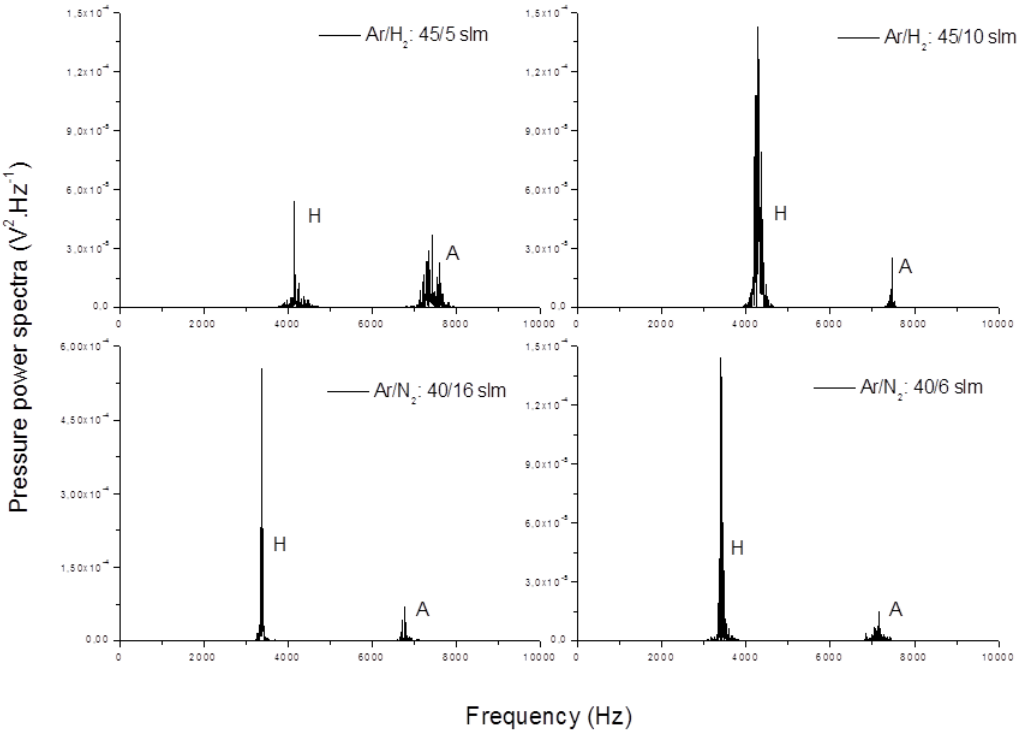

Figure 2.20: Pressure power spectra of filtered arc fluctuations of Helmholtz and acoustic modes for argon-nitrogen and argon-hydrogen plasma.

Moreover, Q factors calculated from voltage power spectra for Ar-H_2 (45-10 slm) and Ar-N_2 (40-16 slm) plasma are, respectively, 30.5 and 97 which highlights stronger Helmholtz resonance when using argon-nitrogen as plasma forming gases mixture. It is confirmed by the results obtained from the pressure power spectra. The standard deviation for Ar-N_2 (40-16 slm) is equal to 68 mbar, which is smaller than the value obtained for Ar-H_2 (45-10 slm), equals 72 mbar. This discrepancy in pressure amplitude can be also explained by a weaker compressibility of plasma forming gases containing nitrogen. In the frame of the mass-spring system model for the Helmholtz resonance, during adiabatic oscillations, the

pressure variation, δp, due to the longitudinal displacement, δx, is given as follows:

$$\delta p = -\gamma_g S P_g \delta x / V_g \tag{2.35}$$

Therefore for the same, δx, smaller pressure amplitude is given by gases with lower isentropic exponent, in this case by Ar-N_2 mixture.

2.2.2.3 Position of the cathode

The model of Helmholtz mode of the instabilities, (2.21), shows that these arc voltage fluctuations are also responsive for the length of the nozzle channel. Therefore, this paragraph presents the examination of the influence of distance between the cathode tip and nozzle exit, L_k, on the resonance of the conventional torch.
The length of the nozzle channel has been varied as presented in Figure 2.21.

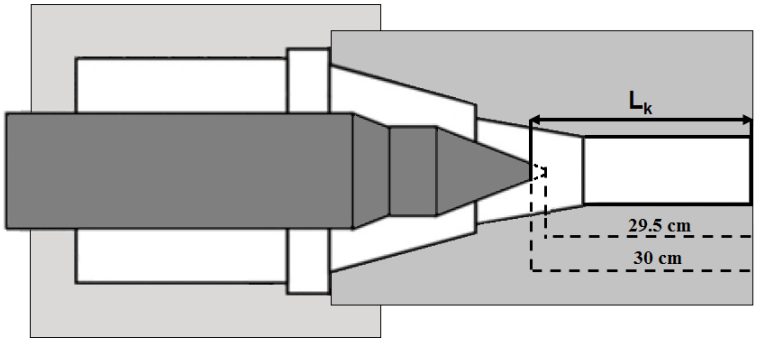

Figure 2.21: Configuration of the torch with identified distance between the cathode tip and nozzle exit, L_k, equals 30 mm and 29.5 mm.

The measurements of the arc voltage and pressure signals have been performed at 400 A for argon-hydrogen (45-10 slm) plasma forming gases mixture by using the torch with the configuration of cathode cavity: (b) V_g = 8.7 cm^3. The signals have been recorded for different L_k, equal to 30 mm and 29.5 mm. The arc voltage and pressure power spectra of the filtered Helmholtz mode computed from the measurements are presented in Figure 2.22 and 2.23.

Table 2.8: The frequency, standard deviation (σ) and Q factor of voltage and pressure power spectra presented in Figure 2.22 and 2.23, for: L_k = 30 mm and 29.5 mm.

	Arc voltage			Pressure		
	f (Hz)	σ (V)	Q	f (Hz)	σ (mbar)	Q
L_k = 30 mm	3500	10	44	3500	13	44
L_k = 29.5 mm	3500	7.5	34.5	3500	9	35

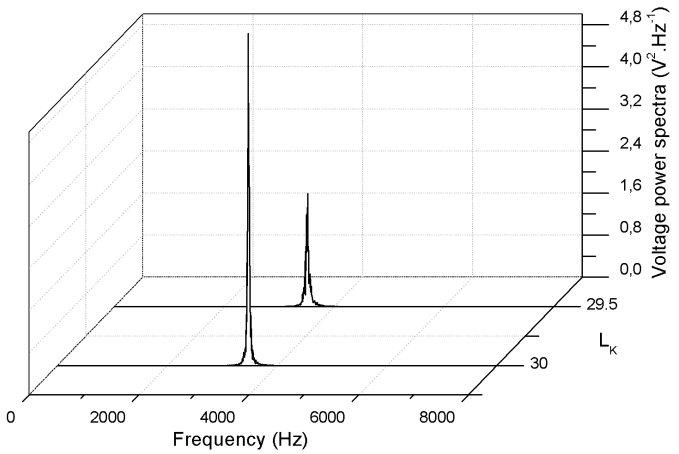

Figure 2.22: Voltage power spectra of filtered Helmholtz mode for L_k: 30 and 29.5 mm [74].

The power spectra and data computed and mentioned in Table 2.8 show that the change of the cathode position does not modify the Helmholtz frequency peak which is approximately 3.5 kHz for both configurations.

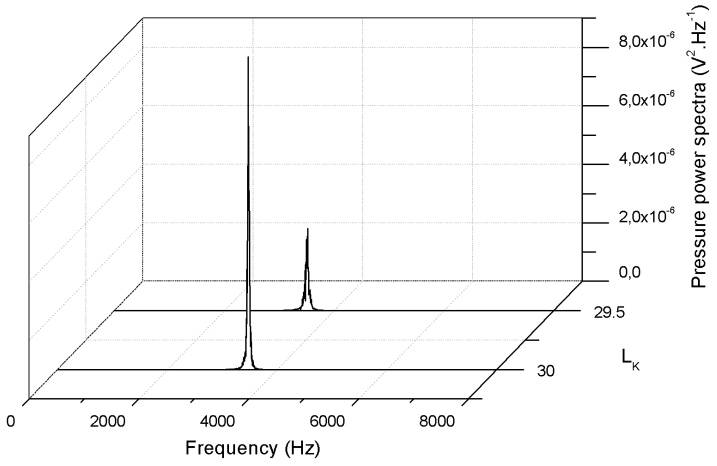

Figure 2.23: Pressure power spectra of filtered Helmholtz mode for L_k: 30 and 29.5 mm [74].

However, a slight decrease of the distance between the cathode tip and nozzle exit, $\Delta L_k =$ 0.5 mm, substantially influences the standard deviation calculated from the arc voltage, 10 V and 7.5 V, respectively, for $L_k = 30$ mm and $L_k = 29.5$ mm.

Moreover, the Q factor of the Helmholtz resonance is changed from 44 for $L_k = 30$ mm to 34.5 for $L_k = 29.5$ mm. Accordingly the cathode position directly affects the Helmholtz resonance, keeping unchanged the mean plasma properties. The cathode position should

influence the turbulence pattern at the entrance of the nozzle and so, by changing the importance of dissipative effects, acts as an adjustable damping parameter.

2.2.2.4 External resonator

To confirm the theory about Helmholtz resonator in the dc plasma torch the external resonator mounted on the cathode cavity has been used. This type of installation allows modifying the pressure waves in the plasma torch, what means that the modification of the pressure inside the cathode cavity leading to the change of arc voltage signal can demonstrate the resonance phenomenon in the torch.

The resonator, presented in Figure 2.24, is composed of a cylindrical cavity (the diameter ϕ_1, in Figure 2.24, equals to 10 ± 0.1mm) and a cylindrical neck (the diameter $\phi_2 = 5 \pm 0.1$mm and the height h $= 6 \pm 0.5$mm) which is connected with the torch cathode cavity.

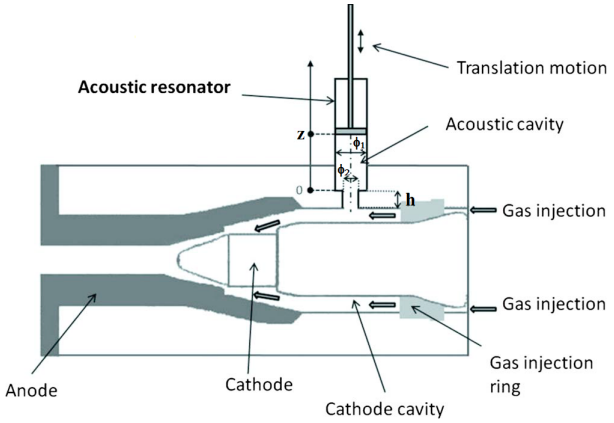

Figure 2.24: Scheme of dc plasma torch with the acoustic resonator [73].

The depth of the resonator cavity is modified using the adjustable position of a piston (referenced with z coordinate). The example of the use of the external resonator is shown in Figure 2.25. The voltage power spectra have been computed from the arc voltage signal obtained for 400 A, for a standard configuration of cathode cavity: case (a) $V_g = 6$ cm^3 and for Ar-N_2 (40-16 slm) plasma forming gases mixture.

The position of a piston z has been changing from 0 mm, which corresponds to closed resonator, to $z_1 = 6$ mm and $z_2 = 8.7$ mm. For z equals 0 mm the power spectrum of the arc voltage signal presents the major peak around 3400 Hz. Comparing the voltage power spectra obtained for different positions of the piston and the standard deviations listed in Table 2.9, the decrease of σ of Helmholtz mode is observed.

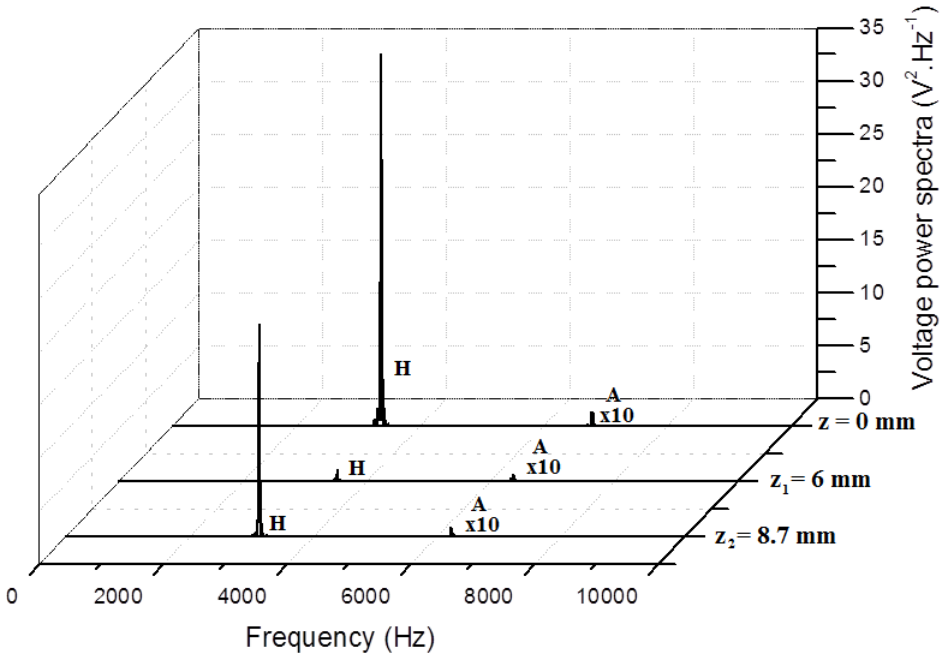

Figure 2.25: Power spectra of arc voltage for different z values obtained for Ar-N_2 (40-16 slm) mixture.

Table 2.9: The frequency, standard deviation (σ) and Q factor of voltage power spectra, presented in Figure 2.25, for z of 0, 6 and 8.7 mm.

		f (Hz)	σ (V)	Q
z = 0 mm	H mode	3400	17	97
	A mode	6800	2.5	33
z = 6 mm	H mode	∼3400	3.8	22
	A mode	∼6400	1.4	22
z = 8.7 mm	H mode	∼3400	11.5	58
	A mode	∼6300	1.3	32

For z = 0 mm the standard deviation and Q factor are, respectively, 17 V and 97, what means that the Helmholtz resonance imposes to the arc a strong oscillatory motion. While increasing the z coordinate σ of Helmholtz peak is decreasing. As it is presented in Figure 2.25 the most effective results are obtained for z_1 = 6 mm. The Helmholtz peak and Q factor are significantly reduced what means that the resonance phenomenon is damped. The influence of the external resonator has been also examined for the arc voltage signal recorded at 400 A for Ar-H_2 (45-10 slm) plasma. Figure 2.26 presents the time-resolved voltage obtained for z_1 = 5.57 mm. To compare the temporal evolution of the signal, from Figure 2.9, measured for the same operating conditions but for the closed resonator, z = 0 mm, is introduced.

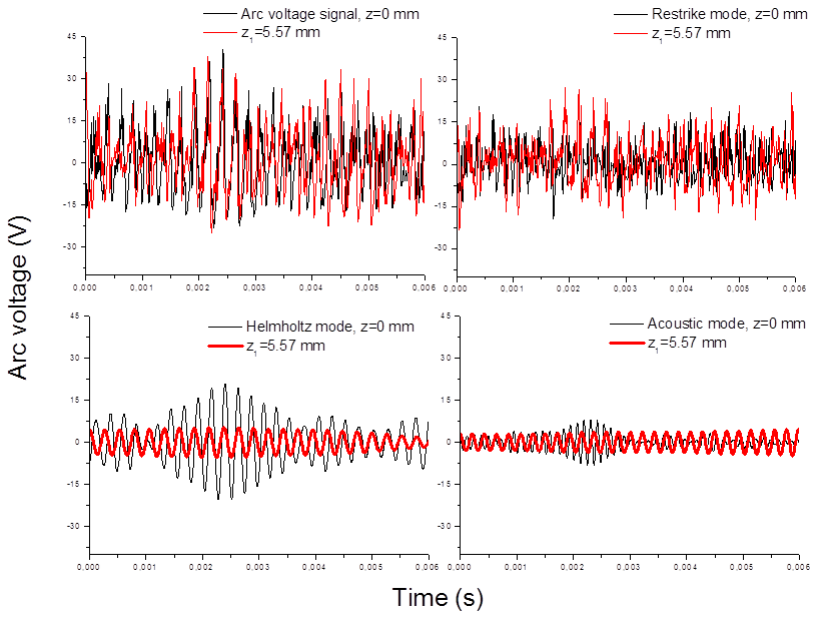

Figure 2.26: Comparison between the arc voltage signal and its filtered components: restrike, Helmholtz and acoustic, measured for closed resonator, z = 0 mm, from Figure 2.9, and the signals obtained for z_1 = 5.57 mm.

The comparison between the results obtained for z = 0 mm and z_1 = 5.57 mm highlights that the amplitude of Helmholtz mode is significantly reduced. Moreover, the resonator has a slight influence on the acoustic and restrike modes.

As the obtained results have shown the use of the external resonator significantly has reduced the arc voltage variations. It is the evidence of a strong coupling between the pressure inside the cathode cavity and the voltage signal. It can be confirmed that the torch nozzle together with the cathode cavity appears to be a Helmholtz resonator. Moreover, the use of the external resonator can be a good method to reduce the plasma instabilities. As the power spectra and the temporal evolution of the fluctuating component of the arc voltage have highlighted typical Helmholtz oscillations can be significantly damped.

In this part of the plasma instabilities studies the Helmholtz and acoustic modes have been investigated. The obtained results have highlighted the the dc plasma torch can behave like the Helmholtz resonator and the frequency of the Helmholtz mode of the plasma oscillations follows the equation:

$$f_H = \frac{1}{2\pi}\sqrt{\frac{\gamma_g P_g}{\rho_p}}\sqrt{\frac{S}{L_p V_g}} \tag{2.36}$$

The measurements of the arc voltage signal and the pressure variations in the cathode cavity have shown the coupling between them what has been confirmed by the use of the

external resonator. Moreover, the results have highlighted the parameters influencing the Helmholtz and acoustic modes. The increase of the cathode cavity volume has noticeably influenced the Helmholtz mode by reducing its frequency. The use of the nitrogen as plasma forming gas has reinforced the Helmholtz mode and dominated the acoustic modes.

2.2.3 Restrike mode

Analysing the temporal evolution of the arc voltage fluctuating component, in Figure 2.27, the regular oscillations with the period of a few hundred μs can be observed, what has been determined as Helmholtz oscillations and studied in the previous paragraphs.

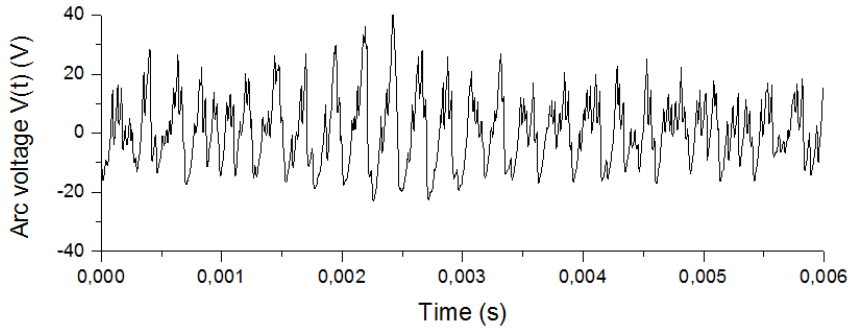

Figure 2.27: Time evolution of the fluctuating component of the arc voltage signal.

Figure 2.27 highlights that to Helmholtz oscillations are superimposed more randomly distributed short events with sharp peaks and sudden falls. The filtering method, Figure 2.9, has underlined that these features, with a mean characteristic time of a few tens of μs, correspond to the restrike mode, i.e. a repetition of the elongation-re-arcing sequences. The model of restrike mode, given in [61], has been presented in chapter 1. It has been determined from the arc voltage signal characterized by pure restrike mode (without the influence of Helmholtz or acoustic modes which depend on the plasma torch geometry). The following section is focused on the examination of the restrike mode in the signal superimposed with the Helmholtz oscillations. The analysis of the restrike fluctuating component, $u_R(t)$, is possible due to the use of the filtering method. The purpose of the following studies is to verify if the restrike component, $u_R(t)$, follows the model presented in chapter 1 [61]. Moreover, the following examinations will be focused on the operating parameters influencing the restrike mode.

As has been presented in Chapter 1, the restrike fluctuations are caused by the elongation of electrical current paths of the arc due to the gas flow until re-arcing phenomena occur through the cold boundary layer, what is presented in Figure 2.28.

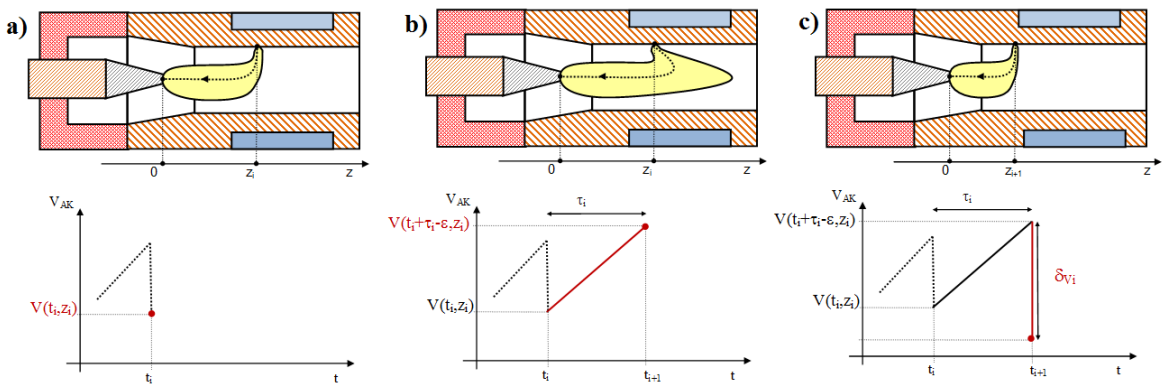

Figure 2.28: Schematic view of restrike model: starting at $t = t_i$ the electrical current path of the arc elongates due to the gas flow, to which corresponds the increase of arc voltage from $V(t_i, z_i)$ to $V(t_i + \tau_i - \varepsilon, z_i)$ (b) during $\tau_i = t_{i+1} - t_i$. Then, a sudden re-arcing occurs at t_{i+1} (c). A new arc is created corresponding to a minimum arc voltage and associated with a voltage jump, δV_i.

The re-arcing occurs from a location of the arc column when the arc voltage, between the arc periphery and the anode wall, exceeds the breakdown threshold, $V_b(z)$, what has been defined in Chapter 1. The voltage drop across the cold layer, $u_{CL}(z,t)$, can also be assumed from Figure 2.29 as follows:

$$u_{CL}(z,t) = u_R(z,t) - u_C(z) \tag{2.37}$$

where $u_C(z) = E_0 z$. E_0 is the electric field through the arc column which is assumed to be constant. The cathode and anode falls are assumed to be also constant during the arc motion and therefore, do not belong to fluctuating component of the signals.

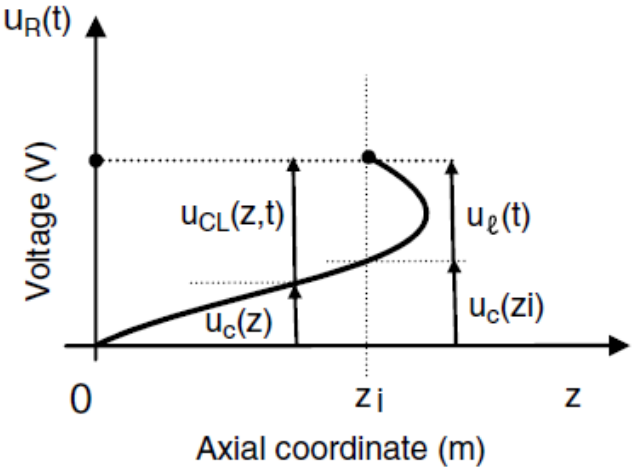

Figure 2.29: Components of restrike arc voltage $u_R(t)$: the voltage drop along the arc column $u_C(z_i)$ which depends on the arc root location, z_i, and the voltage drop along the arc loop, $u_\ell(t)$, which connects the column to the anode wall. The arc voltage presented just after the creation of a new arc root at z_i and at time $t_i + \varepsilon$, $u_\ell(t_i + \varepsilon) = 0$.

When $u_{CL}(z,t) \geq V_b(z)$, a new arc root is created at $z = z_{i+1}$. As has been presented in Chapter 1 and [61] $V_b(z)$ is linked to the thickness of the cold layer, $e_{CL}(z)$. Figure 2.30 shows the evolution of $e_{CL}(z)$.

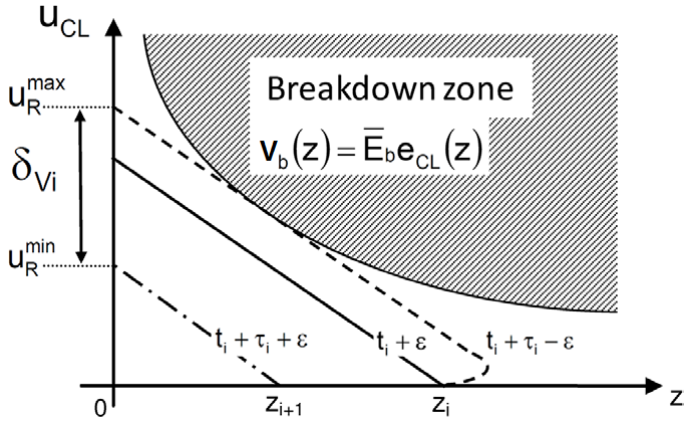

Figure 2.30: Evolution of the voltage drop through the cold layer between the arc column and the anode wall.

At time $t_i + \varepsilon$ just after the formation of an arc root, the arc spot is located at $z = z_i$. The arc current path is elongated by plasma flow during τ_i, u_{CL} increases, and at time $t_i + \tau_i - \varepsilon$, just before re-arcing, u_{CL} reaches the breakdown voltage at $z = z_{i+1}$. Re-arcing occurs and a new arc root is created at a new location, at $z = z_{i+1}$, at time $t_i + \tau_i + \varepsilon$. Therefore, the voltage jump, δV_i, can be defined as follows:

$$\delta V_i(t_i+\tau_i) = u_{CL}(z_i, t_i+\tau_i-\varepsilon) = {u_R}^{max}(t_i+\tau_i-\varepsilon) - {u_R}^{min}(t_i+\tau_i+\varepsilon) = V_b(z_{i+1}) \quad (2.38)$$

If the breakdown zone would be considered as steady, these voltage jumps, δV_i, should be equal. However the turbulences and the instabilities, to which the arc is submitted, have to be taken into account. Therefore, the restrike mode will be considered as a probabilistic process and δV_i will be studied from a statistical point of view, what will be presented below.

The highest values of voltage jumps are obtained for re-arcing occurring close to the cathode. Consequently, for each signal, $u_R(t)$, obtained by the filtering from the raw arc voltage signal, the voltage jumps, $\delta V_i(t_i + \tau_i)$, and their corresponding voltage minima, ${u_R}^{min}(t_i + \tau_i + \varepsilon)$, have been measured. The statistical analysis, which will be presented in the following section, has been obtained from the arc voltage signals measured and shown in the previous paragraphs considering Helmholtz fluctuations but in this section the fluctuating component of the restrike mode obtained by the filtering method will be analyzed.

Figure 2.31 gives the voltage jumps as a function of their corresponding minima for the arc voltage signal obtained at a) 400 A and b) 600 A, for Ar-H_2 (45-10 slm) mixture and the internal nozzle diameter of 6 mm.

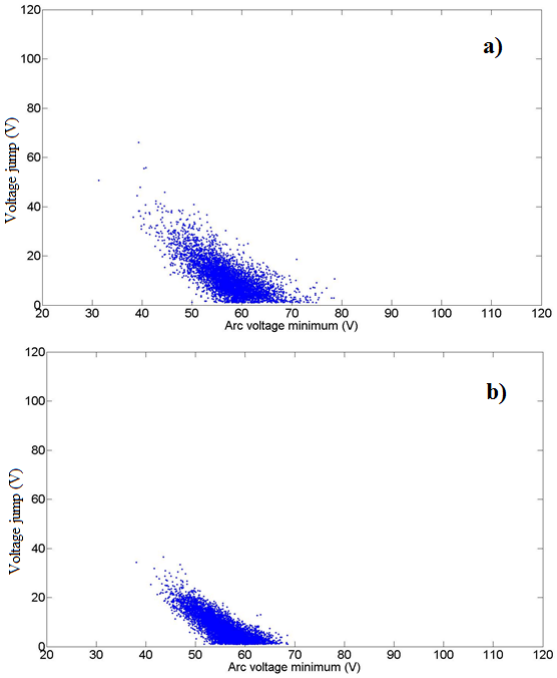

Figure 2.31: Voltage jumps of the fluctuating component as a function of their corresponding minima for the arc voltage signal obtained at a) 400 A and b) 600 A for an internal nozzle diameter of 6 mm, Ar-H_2 (45-10 slm). The mean voltage, $\bar{u}$ = 64.4 V, has been added to ${u_R}^{min}(t_{i+1})$.

The analysis of these data highlights that with the increase of the arc current, the amplitudes of the voltage jumps and the dispersion of the voltage minimum decrease, what is more obviously presented in Figure 2.32. It shows the probability density of voltage jumps calculated for the same measurements as those in Figure 2.31. The number of low amplitude voltage jumps increases as the arc current increases, what is detrimental to the highest amplitude voltage jumps.

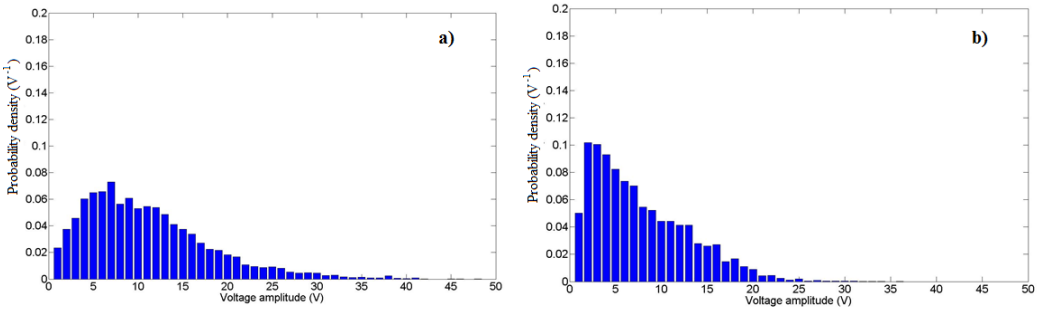

Figure 2.32: Probability density of voltage jump for the arc voltage signal obtained at a) 400 A and b) 600 A for an internal nozzle diameter of 6 mm, Ar-H_2 (45-10 slm).

Figure 2.33 presents the comparison between the voltage jumps computed for the signal measured for the a) Ar-H_2 45-5 slm mixture and b) 45-10 slm. It can be observed that, for a lower H_2 content, the distribution of measurements is shifted to lower values of voltage minima and the dispersion of them is smaller. Moreover, the number of high-amplitude voltage jumps increases as the hydrogen content increases.

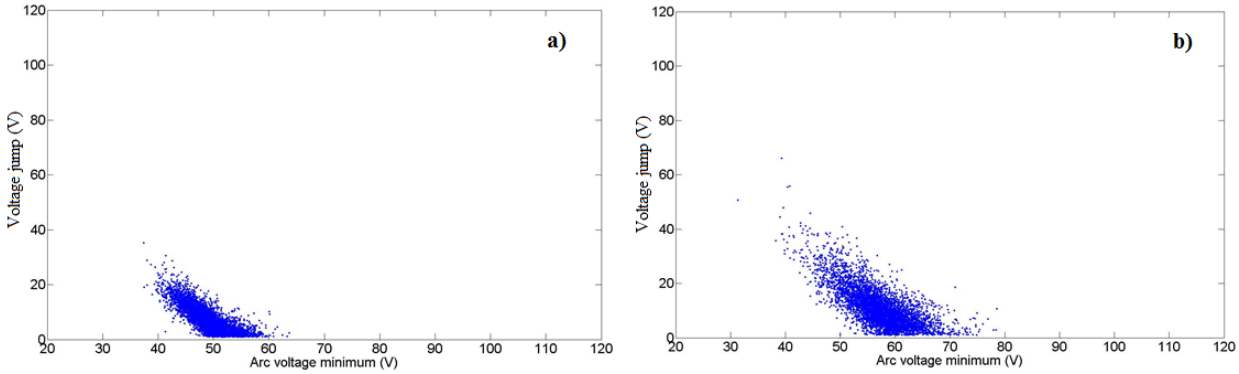

Figure 2.33: Voltage jumps as a function of their corresponding minima for the arc voltage signal obtained at 400 A for Ar-H_2 a) 45-5 slm and b)45-10 slm . The mean voltage has been added to $u_R{}^{min}(t_{i+1})$.

Figure 2.34 presents the mean values of voltage jumps determined from the probability densities of δV_i obtained from the signals measured for different experimental parameters: Ar-H_2 mixtures: 45-5, 45-10 and 45-15 slm and two anode nozzle diameters, 6 and 8 mm, in the function of the arc current.

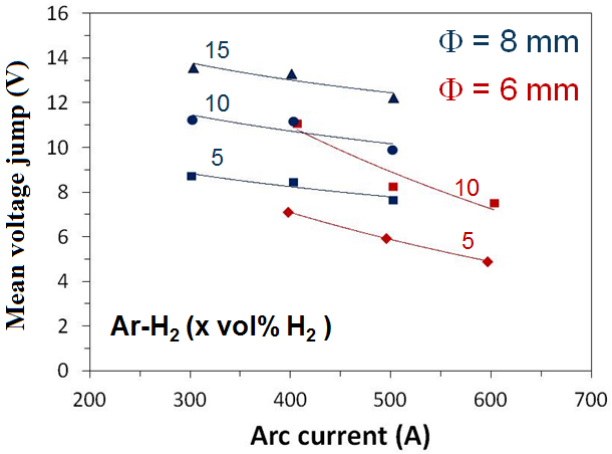

Figure 2.34: Mean voltage jump as function of the arc current for different hydrogen contents in Ar-H_2 mixture x = 5, 10 and 15 slm, and two anode nozzle diameters, 6 and 8 mm.

Figure 2.34 highlights the decrease of mean voltage jumps while the arc current is increasing. Considering the assumptions presented above and taking into account a two-layer model of a stationary axisymmetric arc column in a plasma torch presented in chapter 1, the dependence of mean voltage jumps on operating parameters can be

interpreted in terms of mean thickness of the cold layer, $\bar{e}_{CL}(z)$ and also determine the mean electrical arc radius $\bar{r}_e$. Consequently, as Figure 2.34 highlights the increase of the arc current decreases the mean voltage jumps, what results in the reduction of the thickness of the cold layer, $\bar{e}_{CL}(z)$, and the increase of $\bar{r}_e$. When the hydrogen content is increased from 5 slm to 15 slm, the radial thermal conduction losses are increased, what leads to the decrease of $\bar{r}_e$ and consequently the increase of e_{CL}. Finally, when the internal nozzle diameter increases, e_{CL} also increases. In this case higher voltage jumps are observed, what is due to the decrease of the probability of re-arcing [75].

Figure 2.35 presents the dependence of the mean voltage jumps on the mean cold layer thicknesses for different operating parameters indicated above.

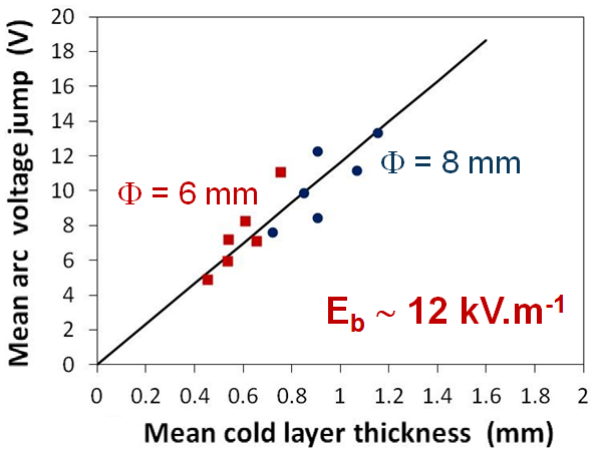

Figure 2.35: Mean voltage jump as function of mean cold layer thickness for different operating parameters: the arc current of 400, 500, 600 A, H_2 content: 5, 10 and 15 slm, and two anode nozzle diameters: 6 and 8 mm [75].

The mean cold layer thickness, $\bar{e}_{CL}$, has been evaluated from the two-layer model presented in chapter 1. The presented quasi-linear dependence allows determining an estimation of the mean breakdown electric field, $\overline{E}_b$, following the restrike model given in chapter 1. $\overline{E}_b$ obtained from the presented experiments is around 12 kVm^{-1}. Up to now, $\overline{E}_b$ has been determined by Paschen's law, which would give the value of $\overline{E}_b$ about two orders of magnitude bigger for the same operating parameters. Therefore, $\overline{E}_b$ may be attributed to the thermal instabilities, what requires more profound studies.

The presented results have verified by the statistical studies that the filtered restrike fluctuating component, $u_R(t)$, follows the model for pure restrike instabilities, given in [61]. It highlights that restrike and Helmholtz modes are relatively separated, what is confirmed by the different times at which they appear: Helmholtz mode at a few hundreds of μs and restrike a few tens of μs. However, the following section will present the different approach to these modes of the instabilities.

2.3 Coupling Helmholtz and restrike modes- "Mosquito mode"

The previous paragraphs have been focused on the studies of the plasma instabilities. As has been presented, the Helmholtz mode appears at the frequency of a few kHz. These oscillations are mainly driven by a cold gas in the cathode cavity, what has been verified by the use of the external resonator mounted on the torch. The frequency of the Helmholtz oscillations, f_H, is defined as follows:

$$f_H = \frac{1}{2\pi}\sqrt{\frac{\gamma_g P_g}{\rho_p}}\sqrt{\frac{S}{L_p V_g}} \tag{2.39}$$

The presented studies of the arc voltage and the pressure signals have highlighted that the increase of the cathode cavity volume can influence the Helmholtz mode by reducing its frequency. Moreover, the use of the nitrogen as plasma forming gas reinforces the Helmholtz mode and dominates the acoustic modes, which, as has been shown, are due to the acoustic waves propagation and reflection inside the torch and occur at higher frequencies ($\sim$ 10 kHz).

The experimental results of the restrike mode can provide the assumption for the mean occurrence frequency of restrike events, f_R, which depends on the probability of re-arcing and on the rate of increase of the arc voltage, as follows:

$$f_R \simeq \frac{1}{\overline{\delta V_i}}\overline{\frac{du_R}{dt}} \tag{2.40}$$

where the rate of increase of the arc voltage, $\overline{\frac{du_R}{dt}}$, presented in Figure 2.28, is proportional to the electric field in the column, E_0, and to the plasma speed, $\overline{v}_p$. The plasma speed has been approximated in the frame of the two-layer model, presented in chapter 1, by the formula:

$$\overline{v}_p = \frac{(\gamma - 1)}{\gamma}\frac{\eta \overline{u} I}{P_a S} \tag{2.41}$$

where S is the nozzle cross section, $\overline{u}$, I and η are respectively measured mean value of the arc voltage, of the arc current and the thermal torch efficiency computed from the energy balance measurements. The presented results of the statistical approach to restrike mode have highlighted the dependence of these fluctuations on the arc current, torch nozzle diameter and flow rate of the plasma forming gas.

As the experimental results have highlighted, the difference between the frequencies of Helmholtz and restrike modes is significant. The Helmholtz mode appears at the time of a few hundreds of μs and the time of the restrike mode equals a few tens of μs, what shows that they are relatively decoupled. However, as the studies of these instabilities have shown, by adjusting the appropriate operating parameters it is possible to influence these two modes.

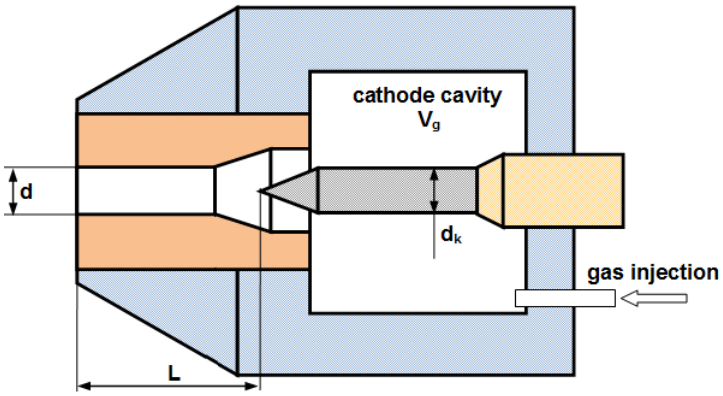

Figure 2.36: Schematic view of a newly designed torch called Mosquitorch.

By increasing the cathode cavity volume, it is possible to noticeably decrease the Helmholtz frequency. Therefore, the obtained results have leaded to the design of a new dc torch with a larger cathode cavity (V_g = 17.8 cm^3), compared to the commercial plasma torches, what is presented in Figure 2.36.

The increase of the cathode cavity has permitted to reinforce the Q factor and to decrease the specific frequency of the Helmholtz mode. Moreover, the longitudinal dimensions of the torch have been shortened to reject the acoustic modes to a higher frequency region. The geometric parameters of the torch as the cathode diameter, d_K, the channel length, L, and the diameter of channel, d, are variable, what is presented in Table 2.10.

Table 2.10: Geometric parameters of a new torch.

Parameter	Value
Cathode diameter d_K (mm)	2.5, 3.5, 4
Channel diameter d (mm)	2.5, 3, 3.5, 4
Channel length L (mm)	10-20

Taking into consideration the parameters influencing and decreasing the frequency of restrike events, the coupling between Helmholtz and restrike modes have been searched experimentally, what is presented in the following paragraph.

2.3.1 Time-resolved measurements of arc voltage

The purpose of these studies is to find the operating parameters which define the most regular temporal variations of the arc voltage. Figure 2.37 presents the arc voltage signals obtained for different experimental conditions. The nitrogen has been used as plasma forming gas due to the possibility to reinforce the Helmholtz mode and dominate the acoustic modes, what has been experimentally presented in the previous paragraphs. The experiments performed above have shown that the frequency of the restrike events depends on the arc current, the diameters of the torch nozzle and the gas flow rate. Therefore, the following studies are focused on the adjustment of these operating parameters.

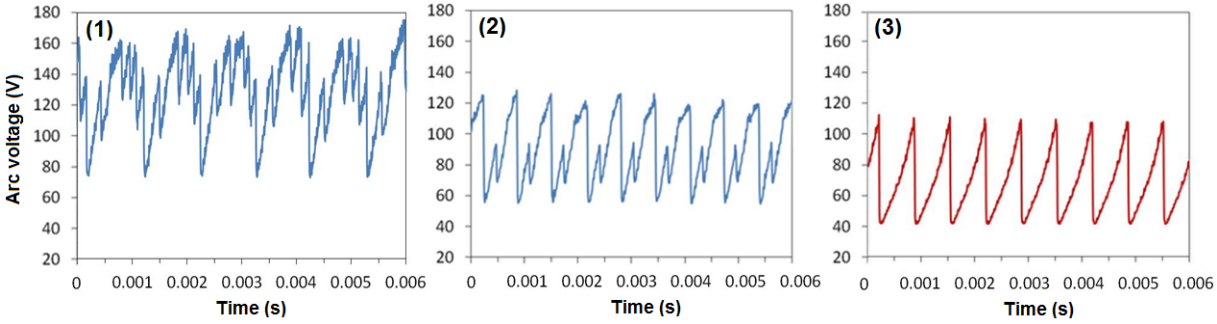

Figure 2.37: Arc voltage signals for different experimental conditions: (1) d_{nozzle} = 3.5 mm, I = 25 A, 2.7 slm N_2, $\overline{V}$ = 129 V, f = 970 Hz; (2) d_{nozzle} = 3.5 mm, I = 10 A, 2.25 slm N_2, $\overline{V}$ = 118 V, f = 1540 Hz; (3) Mosquito mode: d_{nozzle} = 4 mm, I = 15 A, 2 slm N_2, $\overline{V}$ = 73.7 V, f = 1410 Hz [74].

The different nozzles have been tested with the diameters, d, of 3.5 and 4 mm. The torch has been power supplied by the source with regulated arc currents between 8 and 35 A. In Figure 2.37 (1) a typical arc voltage signal, similar to that observed in the conventional plasma torches, has been obtained choosing the nozzle diameter of 3.5 mm, 2.7 slm pure nitrogen and the arc current of 25 A. As can be noticed, this signal is dominated by Helmholtz mode at a frequency close to 1 kHz, shown in Figure 2.38 (1), on which restrike components are superimposed at higher frequencies.

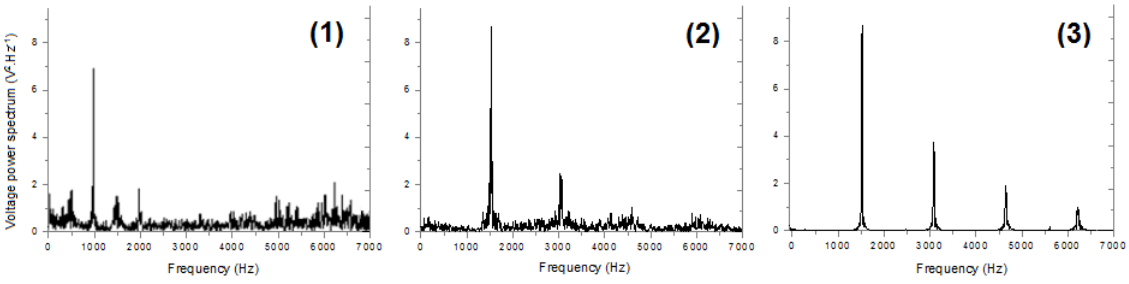

Figure 2.38: Power spectra of the arc voltage signals presented in Figure 2.37.

The decrease of the frequency characteristic for Helmholtz mode is due to the enlargement of the cathode cavity volume and the use of pure nitrogen as plasma forming gas, as has been mentioned above.
The idea is to lower the restrike frequency to approximate this one of Helmholtz and couple these two modes. To define the evolution of the restrike frequency by the operating parameters used in the experiment, the rate of increase in the arc voltage, $(\overline{\mathrm{dV/dt}})$, has been established. To determine $(\overline{\mathrm{dV/dt}})$ the mean slope of the voltage has been measured by the diagnosis of maxima and minima of signals and the calculation of histograms giving the density probability, $\mathrm{p_i}$, of slopes, as follows:

$$(\overline{dV/dt}) = \sum_i (dV/dt)_i p_i \tag{2.42}$$

Figure 2.37 (2) has been obtained by the reduction of the arc current to 10 A and the nitrogen flow rate to 2.25 slm. The nozzle diameter has not been changed and equals 3.5 mm. It is possible to observe a significant decrease of restrike events, which is presented as two patterns per main period (~ 650 μs).
The excepted coupling between the Helmholtz and restrike modes is obtained in Figure 2.37 (3). A very repeatable saw-tooth shape signal has been achieved by increasing the nozzle diameter to 4 mm and the arc current to 15 A, while reducing N_2 mass flow rate to 2 slm. The arc voltage signal is characterized by large and stable amplitude ($67.7\mathrm{V} \pm 2.1\mathrm{V}$). The signal regularity is verified by a low standard deviation of $(\overline{\mathrm{dV/dt}})$, presented in Table 2.11, which gives the mean rate of increases of the arc voltage, $(\overline{\mathrm{dV/dt}})$, and their standard deviations, σ, of all signals: (1), (2) and (3).

Table 2.11: Mean slope of the arc voltage ramps of the signals presented in Figure 2.37.

Figure 2.37	$(\overline{\mathrm{dV/dt}})$ $(10^5\mathrm{Vs}^{-1})$	σ $(10^5\mathrm{Vs}^{-1})$
(1)	2.8594	1.3644
(2)	1.8905	0.3442
(3)	1.0204	0.0411

In case of the arc voltage signal presented in Figure 2.37 (1) the filtering procedure has been used to obtain the separated modes because Helmholtz and restrike are still disconnected. The rate of increase in the arc voltage, $(\overline{\mathrm{dV/dt}})$, what is coupled with restrike frequency, decreases when the nozzle diameter increases, or with the decrease of the arc current either the mass flow rate.

The frequency, 1.4 kHz, of the resonant mode should be the same as that of the Helmholtz mode, which can be written as: $f_H = K_H.\sqrt{\gamma_g P/\rho_p}$ following the model for Helmholtz oscillations. K_H defines the geometric parameters: $\sqrt{S/L_p V_g}$ determined in the equation (2.21). $(\gamma_g P/\rho_p)$ has been calculated as a function of the measured specific enthalpy, h_0, using the database TTWinner [76].

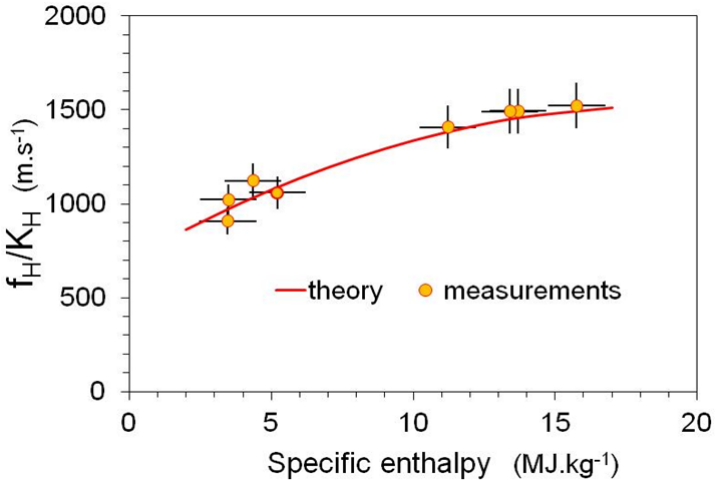

Figure 2.39: Dependence of Helmholtz frequency f_H/K_H on the measured mean specific enthalpy h_0.

Figure 2.39 presents the determination of f_H/K_H as a function of h_0. For a different values of the torch nozzle diameter, d, the arc current, I, and the gas flow rate, q, the frequency f_H has been measured in the range of 1-1.6 kHz with K_H between 0.97 and 1.29 m^{-1}. As Figure 2.39 highlights the obtained results are grouped on a single curve, what shows very good agreement between the experimental and the theoretical values. It confirms that the Helmholtz oscialltions drive the voltage signal in this new regular mode.
When the torch works in this particular mode it emits a stable, sharp and loud sound which resembles the sound produced by a mosquito. Therefore, the term "mosquito mode" has been used to describe the phase locking between Helmholtz and restrike modes.

2.3.2 Enthalpy modulation

To define the stationary characteristics of this periodic plasma jet the energy balance measurements have been carried out. The following section presents the measuring procedures of the mean values of the voltage across the torch (V_{torch} in Figure 2.40), of the arc current (I_{arc}) and the difference of water temperature (ΔT). The obtained results enable to obtain the average specific enthalpy of the plasma jet (h_0), the thermal torch efficiency (η) and the thermal losses at the electrodes in the cooling circuit ($\dot{Q}_{loss}$).

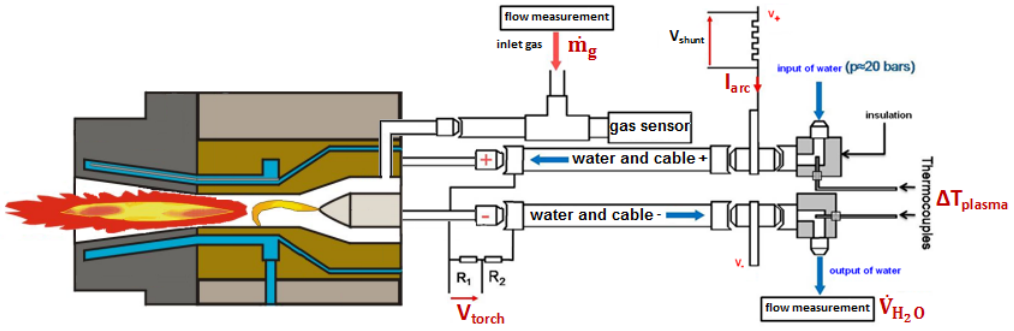

Figure 2.40: Simplified scheme of the energy balance measurements of the torch.

The temperature difference has been measured by two thermocouples type J mounted between the input and the output of the cooling circuit of torch, shown in Figure 2.40. The type J, made by iron-constantan, has been chosen because of its high sensitivity of about 50 μV/°C. The arc current signal is obtained from the voltage drop across the shunt resistor, which is equal to 10^{-3} Ω. The use of shunt resistor allows the measurement of current values too large to be directly measured by the ammeters. In this case the shunt, a manganin resistor of accurately known resistance equals 10^{-3} Ω, is placed in series with the load so that all of the current to be measured will flow through it, shown in Figure 2.40. To make the measurements of the arc voltage the bridge circuit has been implemented, presented in Figure 2.40, with the divider equal to 38.506. Moreover, a new torch uses lower flow rates of the plasma forming gases than in the conventional systems. Therefore, a more accurate measurement of the gas flow has been required. The flow rates have been monitored by a Brooks Instrument SLA5850 mass flow controller (Hatfield, PA, USA) which allows measuring the gas in the range from 0.003 to 30 slpm with the accuracy equals ±1.0% of the rate.

The measurement of ΔT has enabled to determine the thermal losses at the electrodes in the cooling circuit according to the following equation:

$$\dot{Q}_{loss} = \dot{V}.\rho_{water}.C_p.\Delta T \tag{2.43}$$

where:

$\dot{V}$	is the volume flow rate of water circulate in the torch,
ρ_{water}	the density of water,
C_p	the specific heat of water,
ΔT	the temperature difference of water, defined as: $\Delta T = T_{out_{H_2O}} - T_{in_{H_2O}}$

The thermal torch efficiency, η, has been calculated by using the equation:

$$\eta = 1 - \frac{\dot{Q}_{loss}}{V.I} \tag{2.44}$$

where:

V is a measured value of the mean voltage,
I a measured value of the mean arc current.

The electrical power supplied to the torch after removing the heat losses in the cooling circuit is supposed to be converted into enthalpy flux. Neglecting the kinetic energy of the plasma flow, which represents a few per cent of total energy in these conditions, the specific enthalpy can be defined as follows:

$$h_0 = \frac{\eta V I}{\dot{m}_g} \tag{2.45}$$

where:

$\dot{m}_g$ is the total plasma forming gas mass flow rate.

The obtained results of the measurements, performed for the plasma: (1), (2) and (3) in Figure 2.37, are presented in Table 2.12. First of all, it can be noticed that the obtained values of the specific enthalpy are similar to these ones in conventional torches. Moreover, these measurements highlight the use of much lower flow rates of the plasma forming gas comparing to the conventional systems (e.g. Ar-H_2 (45-10 slm) used in the experiments presented in this chapter).

Table 2.12: Energy balance measurements for the case (1), (2) and (3) presented in Figure 2.37.

	d (mm)	I (A)	N_2 (slm)	$\dot{m}$ ($kg.s^{-1}$)	$\overline{U}_{arc}$ (V)	f (Hz)	Q_{loss} (W)	h_0 ($MJkg^{-1}$)
(1)	3.5	25	2.7	5.6×10^{-5}	129	970	854	42
(2)	3.5	10	2.25	4.7×10^{-5}	118	1540	364.5	17.4
(3)	4	15	2	4.2×10^{-5}	73.7	1410	537	13.34

It has been found experimentally that $\dot{Q}_{loss}$ varies almost linearly with the arc current and slightly depends on the nozzle diameter and the gas flow [77, 78]. Therefore, the following part presents the estimation of the specific enthalpy modulation assuming that the thermal losses are constant. This hypothesis permits to determine the equivalent "thermal" voltage, V_{th}, given by: $V_{th} = \dot{Q}_{loss}/I$, where the mean value of the arc current and the thermal losses have been determined above.

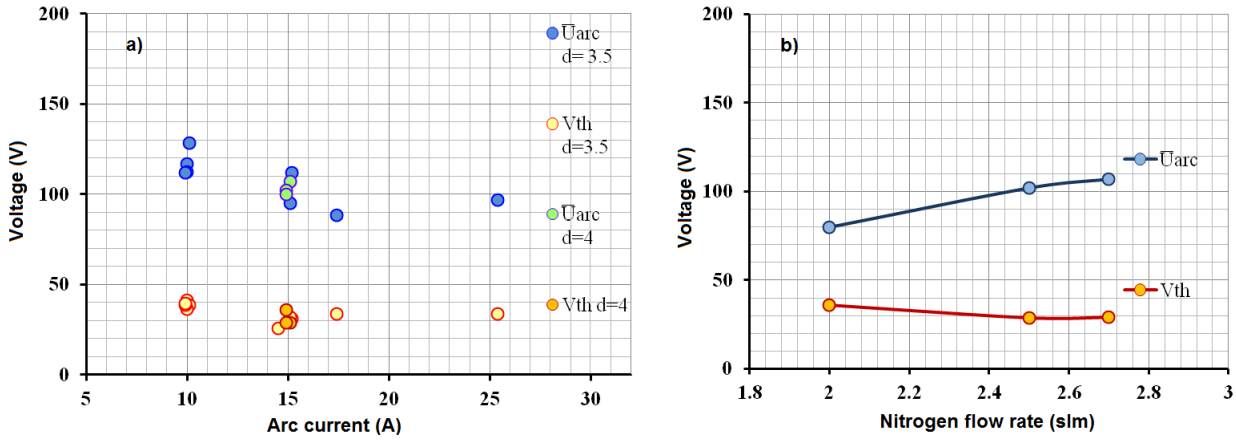

Figure 2.41: Dependence of mean arc voltage and thermal voltage on (a) arc current and (b) nitrogen mass flow rate (b) for different anode nozzle diameters d (mm).

Figure 2.41 presents the measurements of the mean arc voltage, $\overline{U}_{arc}$, and thermal voltage, V_{th}, of the plasma obtained by a new torch. Figure 2.41 a) shows the dependence of $\overline{U}_{arc}$ and V_{th} on the arc current. The measurements have been carried out for two diameters of the torch nozzle: 3.5 and 4 mm. The dispersion of the measurements is related to the fact that for each arc current value different gas flows have been studied. Figure 2.41 b) presents the dependence of $\overline{U}_{arc}$ and V_{th} on the gas flow rates. The results show that the thermal voltage is weakly dependent on the nozzle diameter and gas flow rates.
In case of the plasma jet related to "Mosquito" mode, presented in Figure 2.37 (3) and Table 2.12 (3), the equivalent thermal voltage, V_{th}, can be considered as constant due to high thermal inertia of the heat transfer process through the copper nozzle in comparison with the time variations of arc voltage. V_{th}, calculated from the data listed in Table 2.12 (3), is equal to $\sim$ 36 V. This assumption permits to determine the efficient voltage, which is useful for the conversion of electric power into enthalpy, given as follows:

$$V_{eff} = U(t) - V_{th} \tag{2.46}$$

where U(t) is the arc voltage, presented in Figure 2.37 (3), with U_{min} equals around 40 V and U_{max} around 110 V. Therefore, V_{eff} fluctuates between 4 V and 74 V.
As a consequence, it can be shown that the power supplied to the gas: $P_{el} = V_{eff} \times I$ is modulated in the range 60-1110 W. The variations of the specific enthalpy associated with the efficient voltage fluctuations are given by the following equation:

$$h = \frac{(U(t) - V_{th}).I}{\dot{m}} \tag{2.47}$$

Therefore, the assumed variation of h ranges between 1.4 and 26 $MJkg^{-1}$, what gives the proportion of the enthalpy modulation: $h_{max}/h_{min} \simeq 18$ with a mean value of around 13.3 $MJkg^{-1}$, given by the energy balance measurements (Table 2.12) [74]. Consequently, the temporal variation of temperature, corresponding to given range of enthalpy, should be between 1500 and 7100 K (according to the thermodynamic data found in [17]).

2.4 Conclusions

As has been presented in Chapter 1, the uncontrolled arc plasma instabilities in suspension plasma spraying cause non-homogeneous plasma treatments of material during their flight and also during coatings formation. Therefore, in the framework of this thesis, the modes of plasma fluctuations have been studied in common mono-cathode dc plasma torch. Firstly, the parameters influencing the Helmholtz and acoustic modes have been examined. The presented model of Helmholtz resonance has highlighted that the pressure oscillations in the cathode cavity govern the arc motion. Therefore, the arc voltage signal have been measured simultaneously with the cathode cavity pressure. The obtained results have shown that the Helmholtz resonance strongly depends on the volume of cathode cavity. Moreover, the use of nitrogen as plasma forming gas reinforces the Helmholtz oscillations which dominates the acoustic modes. The studies presented in this part of the chapter have validated experimentally the Helmholtz model and leaded to the assumption of the acoustic resonances representation. Moreover, the investigation of the arc voltage fluctuations have highlighted that the arc motion in dc plasma torch originates, in addition to Helmholtz mode, in the restrike mode. Therefore, the dependence of re-arcing phenomenon on experimental parameters has been highlighted by the statistical measurements. These studies have shown that filtered restrike fluctuations measured from the arc voltage signal coupled with Helmholtz mode follow the model given in [61] for pure restrike fluctuations, which depends on the properties of the cold boundary layer around the arc column. It has highlighted that both modes, Helmholtz and restrike are relatively decoupled. However, the understanding of Helmholtz and restrike phenomena has leaded to a new mode of the arc instabilities. By changing the parameters influencing the Helmholtz and restrike fluctuations, it is possible to couple them together in a newly designed dc plasma torch. Torch working in this new mode emits sharp and stable sound which resembles the sound of the mosquito. Therefore, this mode has been called "Mosquito mode". The energy balance measurements have highlighted that the plasma produced in this new mode is characterized by the enthalpy highly modulated. The properties of this obtained periodic plasma will be used in the following chapter to achieve the suspension injection synchronized with this plasma.

Part II

Résumé du chapitre 2

L'objectif de ce travail est de comprendre les origines des fluctuations de l'arc dans une torche à plasma d'arc conventionnele à courant continu. Les mesures se sont concentrées sur le mode de réamorçage, décrite dans le chapitre 1, et sur le mode Helmholtz récemment mis en évidence. Le but est d'examiner les paramètres de fonctionnement qui influencent ces deux modes. Toutes les mesures ont été réalisées à la pression atmosphérique en utilisant une torche à plasma conçue au laboratoire qui présente une configuration similaire à une torche commerciale F4 (Sulzer Metco, Suisse). La torche est constituée d'une tuyère de diamètre, d, égale 7 mm et la bague d'injection percée de 16 trous de diamètre 1 mm. Le volume de la cavité cathodique, V_g, et la distance entre la pointe de cathode et la sortie de tuyère, L_k, sont variables. Le volume de la cavité cathodique peut être choisi entre: $V_g = 6cm^3$, ce qui correspond au volume standard, $V_g = 8.7cm^3$, obtenue en enlevant la bague d'injection et $V_g = 12.5cm^3$, le volume d'une cavité usinée spécialement dans le laboratoire. L'alimentation de la torche est assurée par une source à thyristors régulée en courant (SNMI, de type P130) qui fournit le courant jusqu'à 1000 A avec une tension maximale de 100 V.

Les mesures résolues en temps des signaux ont été effectuées en utilisant une carte d'acquisition de données (PCI 6132), pilotée par logiciel LabView. Cette carte de National Instruments permet de convertir le signal analogique au format numérique, par échantillonnage et numérisation à l'aide d'un convertisseur analogique-numérique (ADC analog-to-digital converter en anglais). Pour obtenir le signal sans aliasing, le critère d'échantillonnage de Nyquist doit être respecté. Il montre que les échantillons prélevés à une fréquence f_s, doit être supérieure à f_{max} pour obtenir le signal analogique d'origine reconstruit exactement, ce qui est présenté comme suit: $f_s > 2f_{max}$.

Les signaux ont été enregistrés par le programme LabView pour un traitement ultérieur de données, par exemple l'analyse statistique des signaux. Pour atteindre les valeurs fiables, les résultats sont des moyennes de 10 signaux mesurés.

Cependant, l'analyse du signal dans le domaine temporel n'est généralement pas suffisante. Pour étudier toutes les informations que le signal, il est nécessaire de transformer ce signal pour le domaine des fréquences, ce qui peut être fait par la transformation de Fourier FFT. Le résultat de l'analyse FFT est une matrice de nombres complexes, les amplitudes et les phases, ce qui correspond à des oscillations harmoniques élémentaires dans lesquelles le signal peut être décomposé. Les amplitudes correspondent au spectre de puissance, qui indique la quantité d'énergie dans une bande de fréquence donnée ou dans une ligne donnée. Le spectre de fréquence peut être utilisé comme un outil pour distinguer les différents régimes de périodicité et le bruit. Dans le cadre de cette thèse, la transformation de Fourier rapide a été appliquée sous plate-forme LabView.

Les mesures résolues en temps et le traitement des données ont été appliquées au signal de tension d'arc. L'estimation du signal de tension d'arc a été réalisée en utilisant une

carte PCI 6132 d'ordinateur d'acquisition de données, piloté par logiciel Labview, comme cela a été présenté ci-dessus. Cette carte PCI 6132 se compose de 4 entrées analogiques échantillonnées simultanément limitées par la tension au niveau de ±10 V. Par conséquent, pour effectuer les mesures de la tension d'arc un pont diviseur (construit à l'aide de résistances) d'un facteur 22.86 a été implémenté. Comme cela a été présenté ci-dessus, le processus d'échantillonnage est essentiel dans la mesure en temps résolu. En raison de variations rapides des phénomènes re-amorçage dans la torche à plasma (jusqu'à 50 μs), le taux d'échantillonnage de 320 kS/s en 0.2 s a été choisi. Il donne une fréquence d'échantillonnage de 160 kHz, qui répond au critère d'échantillonnage de Nyquist et la résolution de fréquence est égal à environ 5 Hz.
L'évolution temporelle obtenue du signal de tension de d'arc a montré les caractéristiques liées au mode de réamorçage mais superposées à des oscillations plus régulières, pseudo-sinusoidales avec une période d'environ 200 μs. De plus, le spectre de puissance, présenté dans la figure ref FFT2, a mis en évidence la présence d'un pic à ∼4.3 kHz, ce qui ne peut pas correspondre aux fluctuations de restrike, caractérisés par des composantes spectrales non-reproductibles. Les résultats obtenus suggèrent que, dans la torche à plasma à courant continu le mode de réamorçage est superposé sur un autre phénomène. Delair *et al.* ont d'abord suggéré que des oscillations de Helmholtz dans la chambre d'arc pouvaient être la cause des fluctuations de la tension d'arc à hautes fréquences [69]. Cette hypothèse a été proposée car certains systèmes de combustion se comportent comme des résonateurs de Helmholtz [70, 71].
Les variations de la pression dans la cavité cathodique sont générées par l'oscillation du plasma dans le canal de la tuyère, ce qui montre que la cavité de la cathode ainsi que le canal de la tuyère peuvent apparaître comme un résonateur de Helmholtz. L'oscillation de Helmholtz est un phénomène très étudié dans la théorie des vibrations est peut être décrit par analogie par un système masse-ressort.
Le gaz froid dans la cavité cathodique, caractérisée par le volume V_g, est analogue au au ressort, la cavité cathodique constituant alors la cavité du résonateur de Helmholtz.
Cette cavité est connectée au canal de tuyère qui contient le plasma oscillant, analogue à la masse du système masse-ressort. Le plasma oscillant induit une perte de charge due aux frottement et à la turbulence, ce qui ajoute des effets visqueux dans le canal, source de phénomènes non-réversibles. Ensuite, la perturbation de pression dans la cavité de cathode est donnée par l'équation (2.19), où le facteur de qualité, Q, est lié à la bande passante du résonateur, Δf, et au facteur d'amortissement. Par conséquent, la fréquence de Helmholtz liée au mouvement de la masse du plasma dans la tuyère est définie comme:

$$f_H = \frac{1}{2\pi}\sqrt{\frac{\gamma_g P_g}{\rho_p}}\sqrt{\frac{S}{L_p V_g}} \tag{2.48}$$

où: γ_g est le coefficient isentropique du gaz froid, P_g la pression moyenne dans la cavité cathodique, ρ_p la densité du plasma, S est l'aire de la section de la tuyère de la torche, L_p la longueur du canal de buse, V_g le volume de la cavité cathodique. L'équation met en évidence la dépendance du mode de Helmholtz sur les propriétés thermophysiques, γ_g et ρ_p, liées, respectivement, au gaz froid et au plasma, la configuration de la torche, $\sqrt{\mathrm{S/L_p.V_g}}$, et la pression dans la cavité cathodique, ce qui fonction des conditions opératoires et des propriétés thermodynamiques du gaz.
Par conséquent, les études du mode de Helmholtz des oscillations de plasma nécessitent des mesures simultanées de la tension de l'arc et de la pression à l'intérieur de la cavité cathodique.
La pression totale a été mesurée à l'aide d'un capteur piézo-résistif de petite taille (diamètre 4 mm) ENDEVCO 8510C (Meggitt's Endevco, Irvine, Etats-Unis). Le capteur est installé dans la cavité cathodique de la torche. Les mesures simultanées des signaux de la tension de l'arc et de la pression ont été effectuées à l'aide d'une carte d'acquisition de données PCI 6132 pilotée par le logiciel Labview.
L'influence de différentes conditions de fonctionnement sur les oscillations de Helmholtz a été examinée par la mesure des signaux de tension d'arc et la pression à l'intérieur de la cavité cathodique. En outre, les travaux antérieurs du laboratoire ont mis en évidence l'existence d'autres modes de fluctuation due à la propagation des ondes acoustiques [72, 73]. Ces modes, appelés les modes acoustiques, se produisent à des fréquences plus élevées, ∼8.5 kHz. Par conséquent, les expériences présentées ont donné les résultats du mode Helmholtz et des modes acoustiques et du mode de réamorçage (restrike). Pour examiner les oscillations de Helmholtz, acoustique et de réamorçage du plasma, les signaux de ces modes doivent être isolés à partir de la tension d'arc mesurée et de la pression.
La tension d'arc mesurée et la pression peuvent être présentées sous la forme de la somme des modes d'instabilité de jet de plasma: Helmholtz (H), réamorçage (R) ou acoustique (a). Pour observer l'influence de ces modes sur les conditions de fonctionnement, ils ont été isolés à partir du signal, en utilisant le filtre de Wiener numérique programmé sous LabView, définie par la formule 2.27.
Premièrement, les études sur les modes de Helmholtz et acoustique ont été présentées. L'effet de différentes configurations de la cavité cathodique sur ces modes a été examiné. En enlevant l'anneau d'injection, la figure 2.10 (b), et en utilisant la cavité de cathode spécialement usiné, 2.10 (c), trois configurations différentes ont été obtenus avec les volumes : (a)$\mathrm{V_g}$ = 12.5 $\mathrm{cm^3}$, (b) $\mathrm{V_g}$ = 8.7 $\mathrm{cm^3}$ et (c)$\mathrm{V_g}$ = 6 $\mathrm{cm^3}$. Les figures 2.11 et 2.12 présentent les spectres de puissance de la tension et de la pression les composantes des modes Helmholtz (H) et acoustiques (A), filtrées et calculées à partir de la tension d'arc et de pression. Ils ont été enregistrés pour chaque configuration de la cavité de la cathode, pour les mêmes conditions de fonctionnement: $\mathrm{L_k}$ = 30 mm, I = 500 A, Ar-$\mathrm{H_2}$

(45-10 slm). Les résultats présentés dans les figures 2.11 et 2.12 montrent une bonne correspondance entre les modes Helmholtz et acoustiques, et, en outre, entre la tension et la pression. Pour analyser l'évaluation de ces modes les paramètres ont été établis à partir des spectres de puissance et résumées dans le tableau 2.3.
Les écart-types, défini par: $\sigma_i = \sqrt{\langle s_i{}^2 \rangle}$, où s_i sont les signaux de tension ou de pression associés aux modes Helmholtz ou acoustiques, ont été calculés à partir des spectres filtrés par le programme développé sous LabView. Le facteur Q a été établi par l'équation, comme suit: $Q = f_i/\Delta f$, où Δf est la largeur à mi-hauteur mesurée sur les raies Helmholtz ou acoustique dans le spectre de puissance de la tension et de la pression.
Les valeurs de la fréquence de Helmholtz définis à partir des spectres de puissance de la tension et de pression, donnée dans le tableau 22.3, mettent en évidence le décalage des pics f_H à des valeurs plus faibles en raison de l'augmentation du volume de la cavité de cathode, par exemple, de 4500 Hz obtenue pour le cas (c) à 3100 Hz pour (a). Les calculs présentés dans le tableau 2.4 mettent en évidence une bonne compatibilité entre les résultats expérimentaux et le modèle du mode de Helmholtz. Les écarts-types calculées de Helmholtz et modes acoustiques montrent qu'avec l'augmentation du volume de la cavité de cathode, non seulement les fréquences de Helmholtz sont décalées vers des valeurs plus faibles, mais aussi une grande partie de la puissance du signal passe en mode acoustique. Ce phénomène est plus évidemment présenté dans la figure 2.13. Le rapport de puissance, R_i, pour chaque mode de fonctionnement est calculé à partir de la puissance des spectres de tension filtré en programme LabView et tracé en fonction du volume de la cavité de la cathode. Pour le cas (c), où $V_g = 12.5$ cm^3, plus de puissance fluctuante est contenue dans le mode acoustique à l'opposé du cas (a).
En outre, les facteurs Q de résonance de Helmholtz pour la tension de l'arc diminuent également de 30.5 à 19 quand V_g varie de 6 à 12.5 cm^3. Ceci indique que l'énergie de résonance de Helmholtz est transférée à des modes acoustiques.
Les résultats présentés conduisent à rechercher analytiquement les modes acoustiques dans la cavité cathodique en tenant compte des modes radiaux et azimutaux, en plus des modes longitudinaux. La cavité de la cathode peut être supposée être de géométrie cylindrique avec une forme annulaire de longueur L = 38 mm, le rayon intérieur a = 7 mm et le diamètre extérieur b = 10.5 mm. Cette approche analytique compte tenu dans la section "Configuration of the cathode cavity", ont fourni l'équation de modes de résonance des fréquences défini par:

$$f_0 = ({f_{nm}}^2 + {f_\ell}^2)^{0.5} \tag{2.49}$$

où f_ℓ correspond à l'acoustique modes longitudinaux. Le calcul montre que la plupart d'entre eux ont des fréquences supérieures à 10 kHz, sauf le mode (n, m , ℓ) = (1, 1, 1), qui définit:

f_ℓ = 2368 Hz et f_{11} = 6589 Hz, ce qui donne la fréquence f_0 = 7000 Hz. Cette valeur est cohérente avec avec celles mesurées dans les spectres de puissance présentée dans les figures 2.14 et 2.15. En outre, lorsque le volume de la cavité cathodique, V_g, augmente, L présenté dans le modèle (2.32) augmente, ce qui donne la diminution de la fréquence acoustique. Les résultats expérimentaux, énumérés dans le tableau 2.3 et 2.5, montrent la même dépendance.

Dans les études précédentes, présentées dans [72], les mesures des signaux de la tension d'arc et de la pression, obtenues pour des mélanges argon-hydrogène ont été mises en évidence. Les expériences ont été effectuées en utilisant la même torche à plasma. La tension d'arc et la pression dans la cavité cathodique ont été obtenus à 600 A, pour le débit constant d'argon à 45 slm et le débit d'hydrogène variant entre 2 et 10 slm. Les spectres de puissance de tension, présenté sur la figure 2.17 montrent que la composition chimique des gaz plasmagènes influe fortement sur la résonance de Helmholtz, en particulier lorsque le contenu de l'hydrogène est augmentée à mélange binaire comme Ar-H_2. De plus, le débit d'hydrogène doit atteindre un certain seuil, d'environ 5 slm, pour maintenir des oscillations de Helmholtz. Dans la partie suivante, les résultats de l'utilisation de Ar-H_2 et Ar-N_2 sont mis en évidence. Ils ont été obtenus pour les compositions des gaz suivants:

- Ar-H_2 (45-5 slm)
- Ar-H_2 (45-10 slm)
- Ar-N_2 (40-6 slm)
- Ar-N_2 (40-16 slm)

Les mesures de la tension d'arc et de la pression dans la cavité cathodique ont été obtenues à 400 A pour une configuration standard de la cavité: cas (a) $V_g = 6$ cm^3 et pour la distance entre la pointe de cathode et la sortie de la tuyère: L_k = 30 mm. En comparant les motifs des oscillations de la tension d'arc, présentés sur la figure 2.18, obtenue avec le mélange Ar-H_2 (45-10 slm), avec les signaux mesurés pour le plasma argon-azote, un phénomène de battement est observé qui produit des groupes successifs de pics d'amplitudes hautes et basses dans le cas de Ar-H_2 mixture. L'analyse des spectres de puissance de la tension obtenue avec Ar-N_2, représentés sur la figure 2.19, et les données indiquées dans le tableau 2.7 montre que les signaux de tension d'arc contiennent la résonance de Helmholtz sans aucune influence du mode acoustique. Par conséquent, ce phénomène de battement trouvé dans l'évolution temporelle du signal de tension mesurée pour Ar-H_2 (45-10 slm) pourrait être attribuée à un couplage entre les modes de Helmholtz et acoustique. De plus, le spectre de puissance calculé à partir de la tension d'arc (figure 2.19) et la pression de signaux (figure 2.20) mettent en évidence le décalage des pics de fréquence de Helmholtz vers les valeurs inférieures pour plasma argon-azote. La fréquence est égale à 3.4 kHz

pour Ar-N_2 (40-16 slm) plasma et 4.45 kHz pour Ar-H_2 (45-10 slm). L'analyse du modèle de la fréquence de Helmholtz donné dans ((2.21)) montre que cette baisse de la fréquence est dû aux paramètres suivants du plasma Ar-N_2: faible coefficient isentropique, γ, et une densité plus élevée, ρ, comparativement au plasma Ar-H_2.
Le modèle du mode de Helmholtz des instabilités ((2.21)) montre que ces fluctuations de la tension d'arc sont aussi sensibles à la longueur du canal de tuyère. Par conséquent, cette partie présente l'examen de l'influence de la distance entre la pointe de la cathode et de sortie de la buse, L_k, à la résonance de la torche conventionnelle. La longueur du canal de tuyère a été modifiée comme indiqué à la figure 2.21. Les mesures des signaux de tension d'arc et de pression ont été effectuées à 400 A pour le mélange argon-hydrogène (45-10 slm) en utilisant la torche de cavité cathodique: (b) $V_g = 8.7$ cm^3. Les signaux ont été enregistrés pour différentes L_k, égal à 30 mm et 29.5 mm. Les spectres de puissance de tension d'arc et de pression du mode de Helmholtz filtré et calculé à partir des mesures sont présentés sur les figures 2.22 et 2.23. Les spectres de puissance et les données calculées et mentionnées dans le tableau 2.8 montrent que la variation de la position de la cathode ne modifie pas la fréquence de Helmholtz qui est d'environ 3.5 kHz, pour les deux configurations. Toutefois, une légère diminution de la distance entre la pointe de la cathode et de sortie de tuyère, $\Delta L_k = 0.5$ mm, influence sensiblement l'écart-type calculée à partir de la tension d'arc, 10 V et 7.5 V, respectivement, pour L_k = 30 mm et L_k = 29.5 mm.
Pour confirmer la théorie de résonateur de Helmholtz dans une torche plasma à courant continu, un résonateur acoustique externe monté sur la cavité cathodique a été utilisé. Ce type d'installation permet de modifier les ondes de pression dans la torche à plasma, ce qui signifie que la modification de la pression à l'intérieur de la cavité cathodique qui conduit à la modification du signal de tension d'arc peut démontrer le phénomène de résonance dans la torche.
Le résonateur externe est composé d'une cavité cylindrique (le diamètre ϕ_1, illustré sur la figure 2.24, est égal à 110 ± 0.1mm) et un col cylindrique (le diamètre $\phi_2 = 5 \pm 0.1$mm et la hauteur h $= 6 \pm 0.5$mm) qui est relié à la cavité cathodique de la torche. La profondeur de la cavité de résonateur est modifié en utilisant la position d'un piston réglable (référencé avec coordonnée z). L'exemple de l'utilisation du résonateur externe est représenté sur la Figure 2.25. Les spectres de puissance de tension ont été calculés à partir du signal de tension de l'arc obtenu pour 400 A, pour une configuration standard de la cavité de la cathode: cas (a) $V_g = 6$ cm^3 et pour le mélange des gaz Ar-N_2 (40-16 slm).
La position d'un piston z a changé de 0 mm, ce qui correspond à résonateur fermé, par z_1 = 6 mm à $z_2 = 8.7$ mm. Pour z égal à 0 mm, le spectre du signal de tension d'arc électrique présente un pic majeur autour de 3400 Hz. En comparant les spectres de puissance de tension obtenus pour différentes positions du piston et les écarts-types mentionnés dans

le tableau 2.9, une diminution de l'écart type de mode de Helmholtz est observée. Pour z = 0 mm, σ est 17 V, ce qui signifie que la résonance de Helmholtz impose à l'arc une forte oscillation. En augmentant la coordonnée z, σ des fluctuations de Helmholtz diminue. Comme il est présenté sur la figure 2.25, les résultats les plus efficaces sont obtenus pour $z_1 = 6$ mm. Le pic de Helmholtz est considérablement réduit, ce qui signifie que le phénomène de résonance est amorti. Les résultats obtenus ont montré l'utilisation du résonateur externe a considérablement réduit les variations de tension d'arc. C'est la preuve d'un couplage fort entre la pression à l'intérieur de la cavité cathodique et le signal de tension. En outre, l'utilisation du résonateur externe peut être une bonne méthode au réduire les instabilités du plasma puisque les fluctuations de tension peuvent être réduites de façon significative.

La section suivante se concentre sur l'examen du mode de réamorçage superposé aux oscillations de Helmholtz. L'analyse de la composante fluctuante de réamorçage, $u_R(t)$, est possible grâce à l'utilisation de la méthode de filtrage. Le but de ces études suivantes est de vérifier si le composant de réamorçage, $u_R(t)$, suit le modèle présenté dans le chapitre 1 [61]. En outre, les examens suivants seront axés sur les paramètres de fonctionnement qui influencent le mode de réamorçage.

Comme cela a été présenté dans le chapitre 1, les fluctuations de réamorçage sont causées par l'augmentation de la tension d'arc en raison de l'écoulement du gaz. Le processus d'allongement est suivi par un claquage électrique de la couche limite du gaz froid entre la colonne d'arc et la paroi anodique. Un nouveau point d'accrochage est créé en amont de la tuyère, qui correspond à une tension d'arc minimale et qui est identifiée par un saut de tension, ce qui est présenté dans la figure 2.28. La ré-amorçage d'arc se produit à partir de la colonne d'arc lorsque la tension de l'arc, entre la périphérie de l'arc et la paroi de l'anode, est supérieure au seuil de rupture, $V_b(z)$, ce qui a été défini dans la Chapitre 1. La chute de la tension aux bornes de la couche froide, $u_{CL}(z,t)$, peut aussi déduire de la figure 2.29 comme suit:

$$u_{CL}(z,t) = u_R(z,t) - u_C(z) \tag{2.50}$$

où $u_C(z) = E_0 z$. E_0 est le champ électrique à travers la colonne d'arc, qui est supposée être constante. Lorsque $u_{CL}(z,t) \geq V_b(z)$, un nouveau pied d'arc est créé à $z = z_{i+1}$. Comme cela a été présenté dans le chapitre 1, $V_b(z)$ est liée à l'épaisseur de la couche froide, $e_{CL}(z)$ [61]. Figure 2.30 montre l'évolution de $e_{CL}(z)$. Au moment de $t_i + \varepsilon$ juste après la formation du pied d'arc, le spot anodique est situé à $z = z_i$. Le chemin du courant d'arc est allongé par le plasma lors de τ_i, la tension u_{CL} augmente, et au temps $t_i + \tau_i - \varepsilon$, juste avant de re-amorçage, u_{CL} atteint la tension de claquage à $z = z_{i+1}$. Une nouveau pied d'arc est créé dans un nouveau lieu, à $z = z_{i+1}$, au temps $t_i + \tau_i + \varepsilon$. Par conséquent, le saut de tension, δV_i, peut être défini par l'équation (2.38). Cependant, dans ce modèle, les

turbulences et les instabilités de l'arc, doivent être prises en compte. Par conséquent, les arguments ci-dessus doivent être considérés d'un point de vue statistique. Cette analyse statistique a été obtenue à partir des signaux de tension d'arc, le même que dans le cas de l'étude des variations de Helmholtz mais dans ce cas, les études de la composante fluctuante de la mode de réamorçage obtenues par le procédé de filtrage sont présentés.
L'analyse des données a montré que l'augmentation du courant d'arc cause la diminution de l'amplitude des sauts de tension et la diminution de la tension minimum. De plus, pour un plus faible H_2 contenu, la distribution des mesures est décalée vers des valeurs de plus faible de tension. Le nombre desauts de tension à haute amplitude augmente lorsque le contenu de hydrogène augmente. Les résultats présentés sur la figure 2.34 ont montré des valeurs moyennes de sauts de tension déterminées à partir des densités de probabilité de δV_i obtenues à partir des signaux mesurés pour différents paramètres expérimentaux: Ar-H_2 mélanges: 45-5, 45-10 et 45-15 slm et deux diamètres de la tuyère, 6 et 8 mm, en fonction du courant d'arc. Figure 2.34 a mis en évidence la diminution des sauts de tension moyenne tandis que le courant d'arc augmente. Compte tenu d'un modèle à deux couches d'une colonne d'arc stationnaire, axisymétrique dans une torche à plasma présenté dans le chapitre 1, la dépendance des sauts de tension moyenne des paramètres de fonctionnement peut être interprétée en terme d'épaisseur moyenne de la couche froide, $\bar{e}_{CL}(z)$. Le rayon moyen de l'arc électrique $\bar{r}_e$ peut aussi être déterminé. Par conséquent, comme Figure 2.34 met en évidence que l'augmentation du courant d'arc diminue les sauts de tension moyens, ce qui résulte en la réduction de l'épaisseur de la couche froide,$\bar{e}_{CL}(z)$, et l'augmentation de $\bar{r}_e$. Lorsque le débit d'hydrogène est augmenté de 5 slm à 15 slm, les pertes de conduction thermique radiale sont augmentées, ce qui conduit à la diminution de $\bar{r}_e$ et par conséquent l'augmentation de $\bar{e}_{CL}(z)$. Enfin, lorsque le diamètre de la tuyère augmente, $\bar{e}_{CL}(z)$ augmente également. Dans ce cas, les sauts plus élevés de la tension sont observés, ce qui est dû à la diminution de la probabilité de reamorçage [75]. Les résultats présentés ont été vérifiés par les études statistiques que la composante fluctuante filtrée du réamorçage, $u_R(t)$, suit le modèle des instabilités pures du réamorçage, donnés dans [61]. Ils soulignent que le réamorçage et modes de Helmholtz sont relativement séparés, ce qui est confirmé par les différents temps caractéristiques: le mode de Helmholtz à quelques centaines de μs et réamorçage quelques dizaines μs.
En augmentant le volume de la cavité cathodique, il est possible de diminuer notablement la fréquence de Helmholtz. Par conséquent, une nouvelle torche à courant continu a été conçu avec une cavité cathodique plus grande (V_g = 17.8 cm^3), par rapport aux torches à plasma commerciales. L'augmentation de la cavité cathodique a permis de renforcer le facteur Q et de diminuer la fréquence spécifique du mode de Helmholtz. En outre, les dimensions longitudinales de la torche ont été raccourcies pour rejeter les modes acoustiques vers les régions de plus hautes fréquences. En tenant compte des paramètres

d'influence et en diminuant la fréquence des événements de réamorçage, le couplage entre mode Helmholtz et de réamorçage a été recherché expérimentalement. L'azote a été utilisé comme le gaz plasmagène en raison de la possibilité de renforcer le mode de Helmholtz et dominer les modes acoustiques. En outre, la fréquence des événements de réamorçage dépend du courant d'arc, le diamètre de la buse de la torche et de la vitesse d'écoulement du gaz. Par conséquent, les études ont été concentrées sur le réglage de ces paramètres de fonctionnement. Différentes tuyères ont été testées avec un diamètre, d, variant de 3.5 et 4 mm. Le courant d'arc a été modifié de 25 A à 15 A. Le débit d'azote a été choisi de 2.7 slm à 2 slm. Le couplage entre les modes de Helmholtz et réamorçage a été obtenu pour le courant d'arc de 15 A, le diamètre diamètre de tuyèrede 4 mm et le débit d'azote de 2 slm, présenté sur la figure 2.37 (3). Le signal de tension d'arc obtenue dans ce nouveau mode est très reproductible en forme de dents de scie, caractérisée par une amplitude importante et stable ($67.7\text{V} \pm 2.1\text{V}$), à la fréquence de 1.4 kHz. Lorsque la torche fonctionne dans ce mode particulier, il émet un son stable, fort et bruyant qui ressemble au son produit par un moustique. Par conséquent, le terme "mosquito mode" a été utilisé pour décrire ce nouveau mode de couplage entre les modes de Helmholtz et réamorçage. Les mesures de bilans d'énergie ont permis de définir l'enthalpie spécifique, h, du plasma produit dans ce nouveau mode. Les variations de h ont été obtenues, comprise entre 1.4 et 26 MJkg^{-1} en considérant constantes les pertes thermiques aux électrodes. Il donne la proportion de la modulation d'enthalpie: $h_{max}/h_{min} \simeq 18$ avec une valeur moyenne d'environ 13.3 MJkg^{-1}. Par conséquent, la variation temporelle de la température, ce qui correspond à l'enthalpie modulée, doit être comprise entre 1500 et 7100 K (d'après les données thermodynamiques trouvés dans [17]).